Thermal Protection System P50 Cork Environments and Response due to Radiative Heating

Manish Mehta[1*], David A. Brewer[1†], Ron D. Beshears[1‡], Guy C. McDougal[1§], Elizabeth S. Schofield[1**]

[1]*NASA Marshall Space Flight Center, Huntsville, Alabama, 35812*

Space Launch System (SLS) experienced deflagration of the acreage of the Core Stage base heat shield during the Green Run hot-fire test campaigns and Artemis I flight. The burning products from the base heat shield during Green Run hot-fire test operation led to concerns in aerothermal environments and thermal protection system (TPS) performance prior to Artemis I flight. This work documents a highly controlled ground test within the NASA Marshall Space Flight Center's Nonmetallic Materials Branch thermal vacuum chamber (TVC) and investigates the P50 cork heat transfer environments and thermal protection system (TPS) response due to sensitivity changes in radiative heat rates, ambient pressure, air entrainment mass flow rates, test gas and TPS sample types. An SLS ascent ambient pressure profile was also simulated within the TVC facility. This test data enabled the efforts toward the Artemis I SLS post-flight reconstruction and initial assessment of flight TPS performance. A ground test program was developed to gain an in-depth understanding of the cork combustion dynamics and TPS response due to the SLS launch vehicle flight ascent environments.

Nomenclature

Al	=	Aluminum
APP	=	TVC Operational Algorithm
BHS	=	base heat shield
BFS	=	BTU/ft^2-sec
BET	=	best estimated trajectory
CFD	=	computational fluid dynamics
CS	=	SLS core-stage
CT	=	computed tomography
DFI	=	Development Flight Instrumentation
GTP	=	gas temperature probe
HD	=	high definition
HF	=	Green Run Hot-Fire Test
P	=	pressure
P50	=	Phenolic resin cork with 50 *u*m granules
R	=	gas constant
*qdot*r	=	radiative heat flux
SLS	=	Space Launch System
SRB	=	Solid Rocket Booster
T+	=	SLS lift-off time or test start time
T	=	temperature
t	=	time
TC	=	thermocouple
TVC	=	thermal vacuum chamber
TPS	=	thermal protection system
V	=	thermal vacuum chamber volume

[*] Subject Matter Expert (SME), Aerosciences Branch, AIAA Senior Member, manish.mehta@nasa.gov
[†] Aerospace Engineer, Aerosciences Branch
[‡] Subject Matter Expert (SME), Damage Tolerance Assessment Branch
[§] Sr. Engineering Specialist, Nonmetallic Materials and Space Environmental Effects Branch
[**] Subject Matter Expert (SME), Nonmetallic Materials and Space Environmental Effects Branch, Amentum/ESSCA, AIAA Member

I. Introduction

Artemis I was the first human-rated lunar system test flight since Apollo 5 in 1968 where the Saturn V launch vehicle carried the Service, Lunar, and Command Modules around the moon[1-3]. Artemis I was the first integrated test flight encompassing the Space Launch System (SLS) launch vehicle and the Orion spacecraft. Artemis I successfully launched from Pad39B from the Kennedy Space Center, Florida on November 16, 2022, as shown in Figure 1. The SLS was propelled with four liquid hydrogen (LH_2) and liquid oxygen (LO_2) rocket engines and two five-segment solid rocket boosters (SRB)[1-3].

There were various base components for the SLS vehicle that were instrumental in protecting the base of the vehicle from excess heating during flight. The base heat shield (BHS) which is the largest aft-end acreage structure, protects the base of the vehicle and its internal components and avionics cabling from excessive rocket plume-induced heating. Boeing was using P50 cork for the BHS which was coated with Hypalon paint. The engine-mounted heat shield (EMHS) protects RS-25 turbopump machinery and gimbal actuators. A thermal blanket was used for the EMHS. Thermal protection systems on the aft end are needed due to the high thermal environments experienced on ascent due to multi-engine launch vehicle operations.

Figure 1 shows the Artemis I flight core-stage and SRB base region with all first-stage engines and solid rocket motors firing nominally. The complex flow field can be seen with six rocket exhaust plumes and atmospheric air interacting in the SLS Core Stage and SRB base regions at T + 15 seconds. The T + 0 second point for Artemis I flight data analysis was defined at SRB ignition which occurred on November 16th, 2022, at 1:47:44 AM EST. All flight time in this report was with respect to this reference time. The SRB aluminum-oxide laden plumes were bright (near saturated pixels) while the RS-25 water vapor dominated plumes were relatively transparent. Along with the complex plume flow field, there was two-phase TPS – gas phenomena occurring on the surface of the heat shield during ascent which will be described in detail within this paper. This infrared (IR) imagery data (Figure 1) was captured by the MARS Scientific ground-based imager system which was part of the NASA Langley Research Center's Scientifically Calibrated In-Flight Imagery (SCIFLI) Team[4].

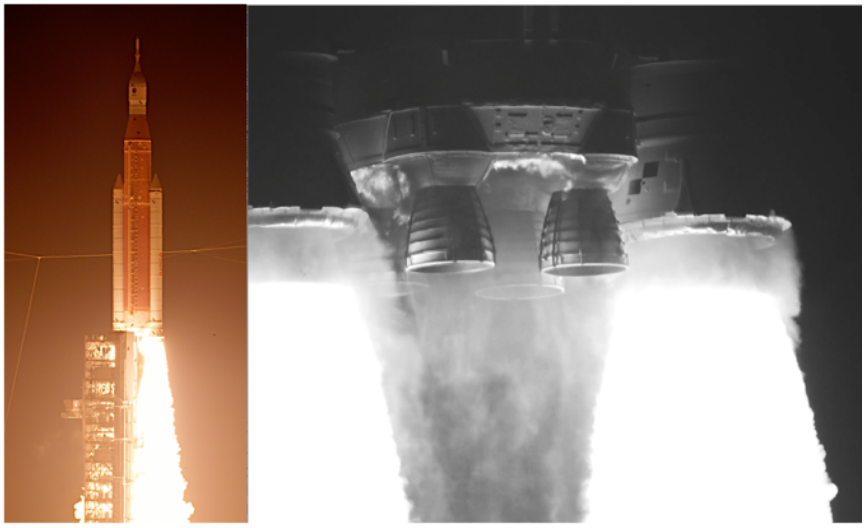

Figure 1. Artemis I SLS launch (left) and IR image of the SLS base at T+15 seconds (right).

Figure 2 shows a large-scale combustion phenomena on the base heat shield which was first uncovered during SLS Core Stage Green Run Hot-Fire Test 1 and Hot-Fire Test 2 test series at flight-scales[5]. The cork combustion dynamics were first observed in 2017 through visible imagery in some pre-cursor sea-level sub-scale ground tests at the NASA Marshall Space Flight Center's Nonmetallic Materials and Space Environmental Effects Branch Thermal Vacuum Chamber (TVC) in support of the SLS Green Run tests[5]. Cork combustion was also observed during Titan IV Stage TPS testing[6]. The base heat shield experienced active burning for a long duration, leading to large plume induced radiation and convection heat loads and subsequent extensive charring of the TPS as shown in Figure 3. It was not anticipated that the foil (covering the P50 cork to minimize radiative heating) would liberate and that the base TPS fire intrusion would delaminate large acreage of foil. As predicted from the pre-flight models[7], this large-scale

combustion process was also observed on the foil-less base heat shield during Artemis I flight from ~T+10 seconds to ~T+75 seconds[1]. This is based on flight instrumentation data and indirect inference of the phenomena. Visual imagery of SLS ascent base region terminated at T+43 sec. Based on Artemis I post-flight reconstruction, this regime led to the largest convective heating environments on the vehicle as predicted by the pre-flight models[7]. It was concluded that P50 cork combustion led to a large deflagration along the full acreage of the base with (Green Run) or without (Artemis I flight) the foil covering[1,2,5] as shown in Figure 2.

The primary objective of this paper was to characterize and understand the P50 cork combustion dynamics and material response to best assess catalytic heating environments during SLS ascent. The main focus of this investigation was to understand the various sensitivities that lead to cork ignition and flame out, the flame dynamics and convective and radiative heating environments. This would lead to the enabling of more accurate base heating design environments prior to Artemis II, the first crewed Artemis flight to the moon. Although the Core Stage Green Run[5] static hot-fire campaign, completed at the B-2 test stand at Stennis Space Center, first provided a glimpse of these cork combustion environments on the base heat shield and aft end (Figures 2 and 3), various dynamics of this combustion process were largely unexplored. The characterization was done by ground testing completed at the NASA MSFC's TVC. The flight base heat shield TPS performance did not provide substantiating data, as it was not instrumented with backside, or substrate thermal couples, and the vehicle was expendable. Internal RS-25 thermal couples were the only means to determine intercompartment temperatures. However, controlled ground tests gave means to simulate the pressure-altitude and induced heat flux leading to the combustion phenomena and substantiating thermal data to further assess TPS performance. Through ground and airborne imagery assets that track the flight path, the goal was to assess the ability to remotely measure TPS surface temperature with sufficient accuracy to be useful[4].

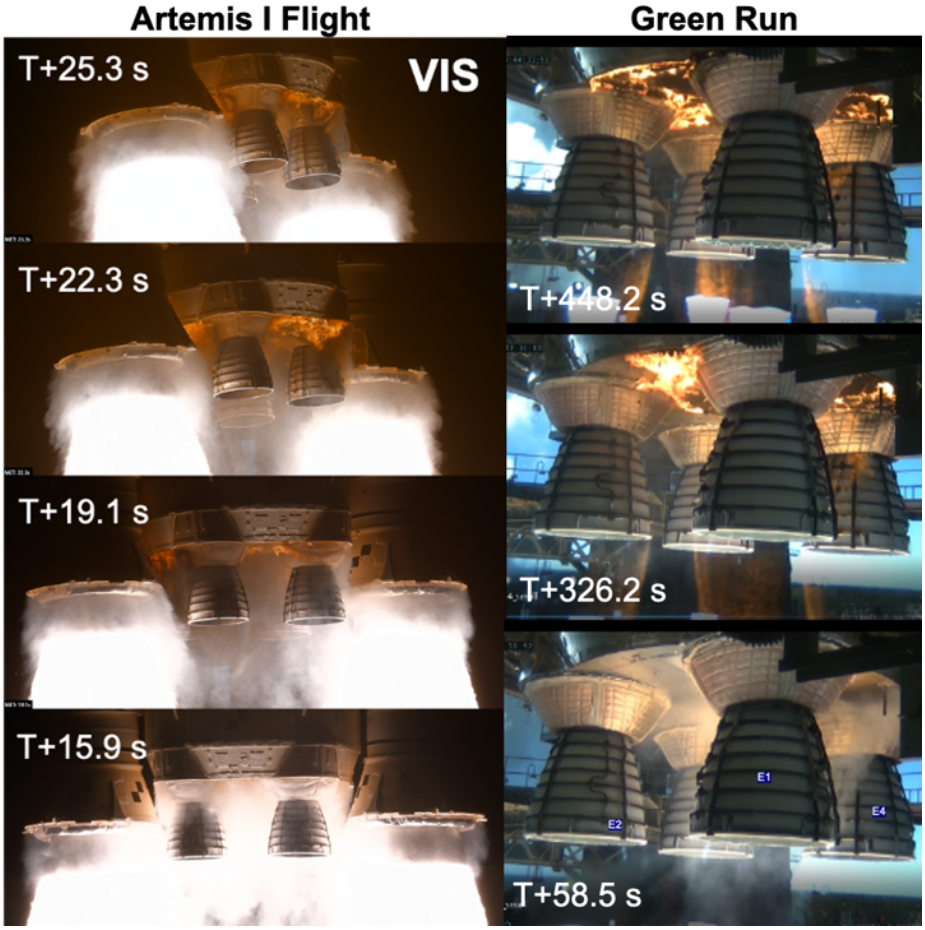

Figure 2. Artemis I (left) and Green Run (right) SLS Core Stage base heat shield TPS cork combustion phenomena[1-2,5].

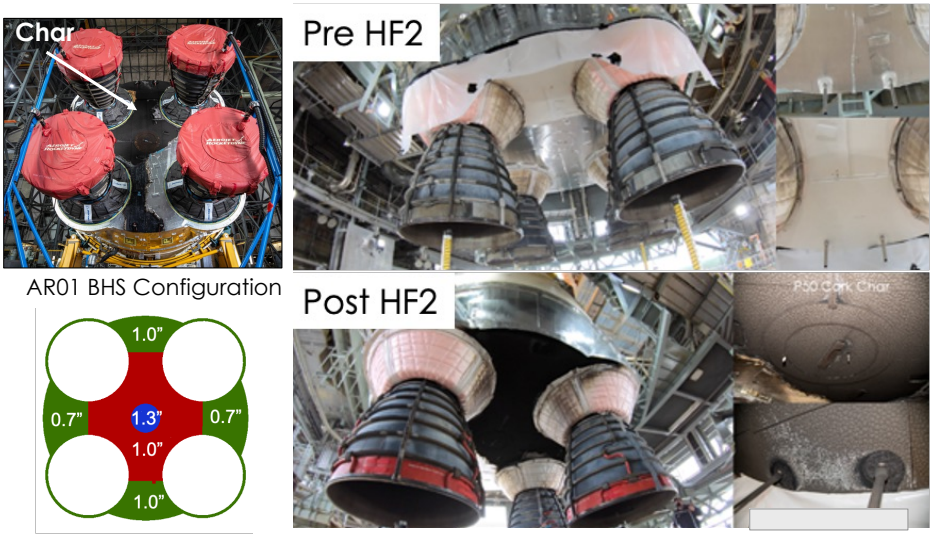

Figure 3. Extensive Green Run SLS Core Stage base heat shield TPS charring[5].

II. Methodology

A. Thermal Vacuum Chamber (TVC) Radiative Heating Testing

Tests of the P50 cork to characterize the radiative heating environment were conducted in a NASA MSFC TVC. This facility was a vacuum chamber with radiant arc lamps that provide radiant heating from 2 BFS to 12 BFS and can reduce ambient pressure from sea-level to 1.9 psia at various set points. The ability to dynamically ramp down the ambient pressure in the TVC provided the capability to simulate the launch vehicle ascent profile. Test durations of up to 100 seconds can be conducted, depending on the imposed radiant heat rate and the lamp cooling water mass flow rates. Optical window access with high resolution visible imagery was also available. Tests in the TVC showed evidence of P50 cork combustion phenomena (Figure 4) in an early test series in 2017, which led to the application of the protective Nexolve tape to the base heat shield prior to the Green Run[2]. A calibration plate was always installed to make sure that the target conditions was satisfied prior to introducing a TPS test panel as shown in Figure 4.

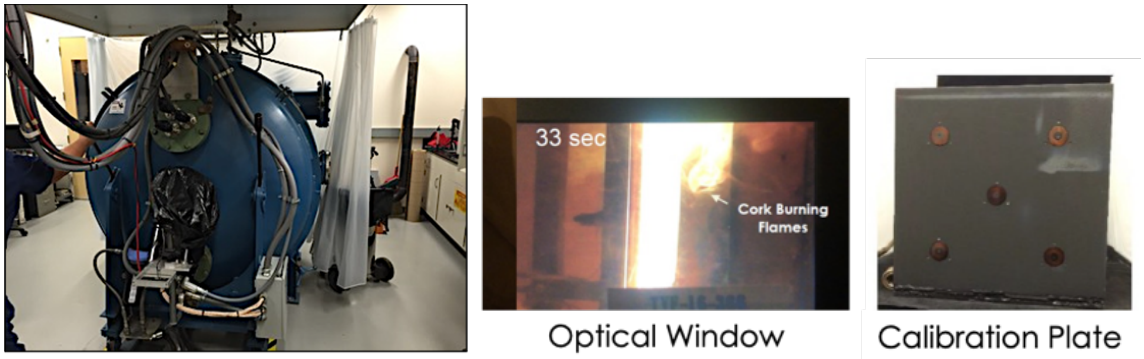

Figure 4. Radiative heating thermal vacuum chamber (left) thermal vacuum chamber optical window (middle) and calibration plate (right).

There were many other components of the TVC for the radiative heating test campaign. As shown in Figure 5, an air inlet (capable of accommodating up to 125 psig compressed air) was used to introduce an entrained air flow rate characteristic of ascent environments. There was a high-definition (HD) camera within the optical port window. As shown in Figure 5, the 30 quartz lamps outputs about 90,000 Watts of radiant heat. As shown in Figure 6, the lamp radiant heat direction was orthogonal to the TPS sample, and the entrained air flow direction is shown in blue. Only 11” x 11’ TPS samples could be installed within the TVC.

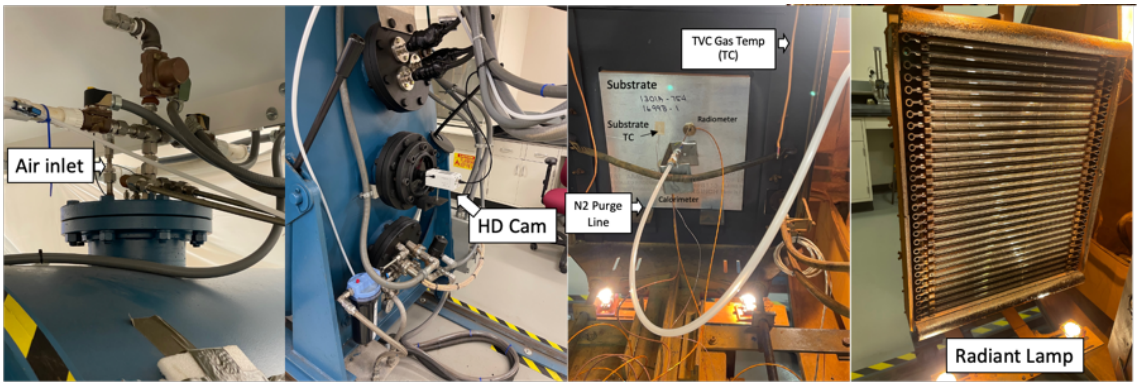

Figure 5. Thermal vacuum chamber radiative heating components.

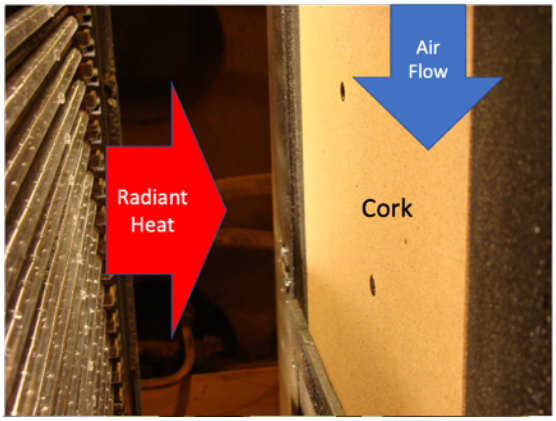

Figure 6. TPS sample positioning within the thermal vacuum chamber radiative heating test.

B. Test Instrumentation

Two MEDTHERM[8] heat flux sensors were embedded in the TPS for the TVC test campaign. One calorimeter and one radiometer were mounted flush with the P50 cork panel at the locations shown in Figure 7. The calorimeter measured the total heat flux applied to the sensor head element. The radiometer measured the radiative heat flux to the sensor head element. A sapphire window over the radiometer sensor head disables the measurement of the convective heating component to only allow the measurement of the infrared spectral band radiation component. The radiometer had a field of view of 150 deg and the calorimeter had a view of 180 deg and both measurements were down sampled at a sampling rate of 10 Hz. The stem of the calorimeter was 1.15” long with a diameter of 0.375” as shown in Figure 8. The radiometer had a length of 1.15” with 0.375” diameter. Subtracting both measurements when temporally synchronized provided an estimate of the convective heat flux to the TPS panel. It should be noted that a correction to the radiometer raw data was needed to be done to account for the differences in FOV between the calorimeter and radiometer. This led to approximately 7% artificial increase in the radiative heating. The instrumentation installation and specifications on the TVC TPS panels were similar to those of the developmental flight instrumentation (DFI) for Artemis I on the Core Stage base heat shield (Figure 7) and for to those to be implemented on the Artemis II mission. These sensors provided local TPS surface total, convective and radiant heat flux environments during the test operation while subjecting the TPS sample to radiant heating. The radiometer had a nitrogen purged line to remove potential soot deposits on the sapphire window and minimize erroneous measurements. The calorimeter had a Type K thermocouple to provide a reference wall temperature in backing out the heat transfer coefficient. A gas temperature probe was not installed within this ground test panel as completed for the Core Stage base heat shield as shown in Figure 7. However, a thermocouple wire exposed to the freestream was installed within the TVC test to record a qualitative gas temperature measurement. This sensor was freely hanging on the backside of the TPS plate as shown in Figure 5. A substrate backside Type K thermocouple was included as well.

The calibration plate shown in Figure 9 contained 5 water-cooled Schmidt-Boelter calorimeters to ensure adequate target total heating environments are obtained from the radiant heating lamps. This facility simulated launch vehicle ascent environments and targeted the total heating rates, entrained air mass flow rates and ambient pressure. These were the drivers to simulate TPS response and associated environments. Below in Figure 9 is a layout for the 11" x 11" calibration plate that contained 5 water-cooled surface calorimeters. The TPS panel was positioned orthogonally to the radiant arc lamps. The calibration plate test runs were conducted before and after each TPS sample test to confirm successful operations of the embedded TPS instrumentation.

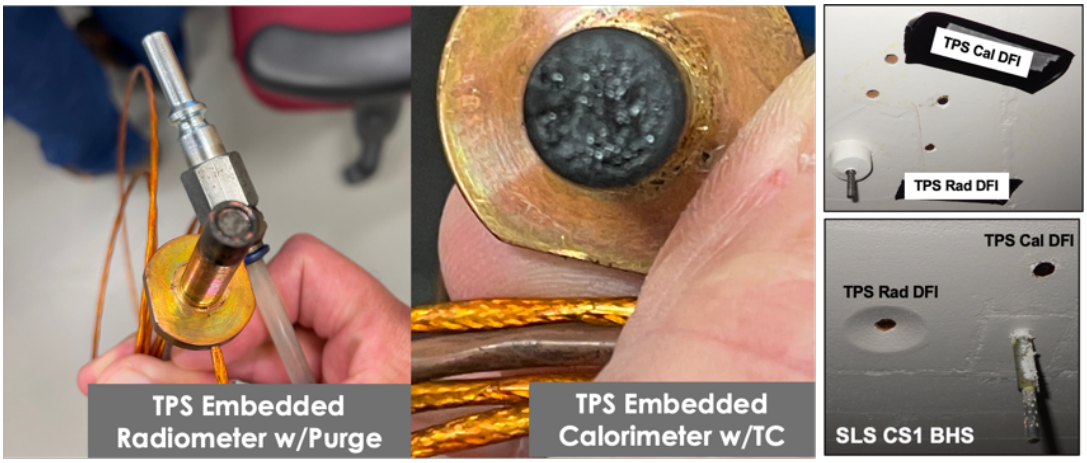

Figure 7. TPS embedded radiometer and calorimeter for the TVC ground test (left) and on the Artemis I SLS Core Stage base heat shield.

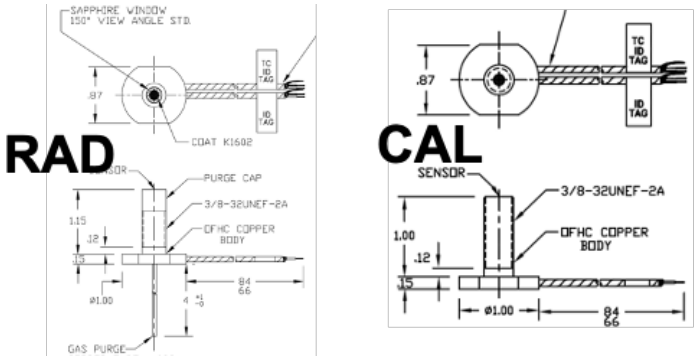

Figure 8. Engineering drawing of the TPS embedded MEDTHERM radiometer and calorimeter for the TVC ground test[8].

C. Thermal Protection System Samples

The TPS samples characterized included both the uncoated and Hypalon-coated P50 cork panels. Below is the TPS stack-up for the SLS Core Stage base heat shield and the TVC test campaigns. It could be seen in Figure 9 that the stack-up for the ground test was similar to flight in material and thickness. The one difference was the substrate thickness was marginally larger for the TVC test campaign compared to the base heat shield. White Hypalon paint (shown in Figure 9) was coated over the bare P50 cork panels at the Michoud Assembly Facility in New Orleans, Louisiana and delivered to Marshall Space Flight Center for testing. Figure 9 shows pictures of the calibration plate, P50 cork panel and Hypalon-coated P50 cork panel. Two holes for the embedded instrumentation were introduced

into all the TPS panels before TVC testing. Hypalon paint was added to minimize moisture and fungal growth that could impregnate the cork and potentially alter the TPS performance during flight. The embedded calorimeter and radiometer were removed for the TPS samples that were transferred to the MSFC Hot-Gas Facility for further testing.

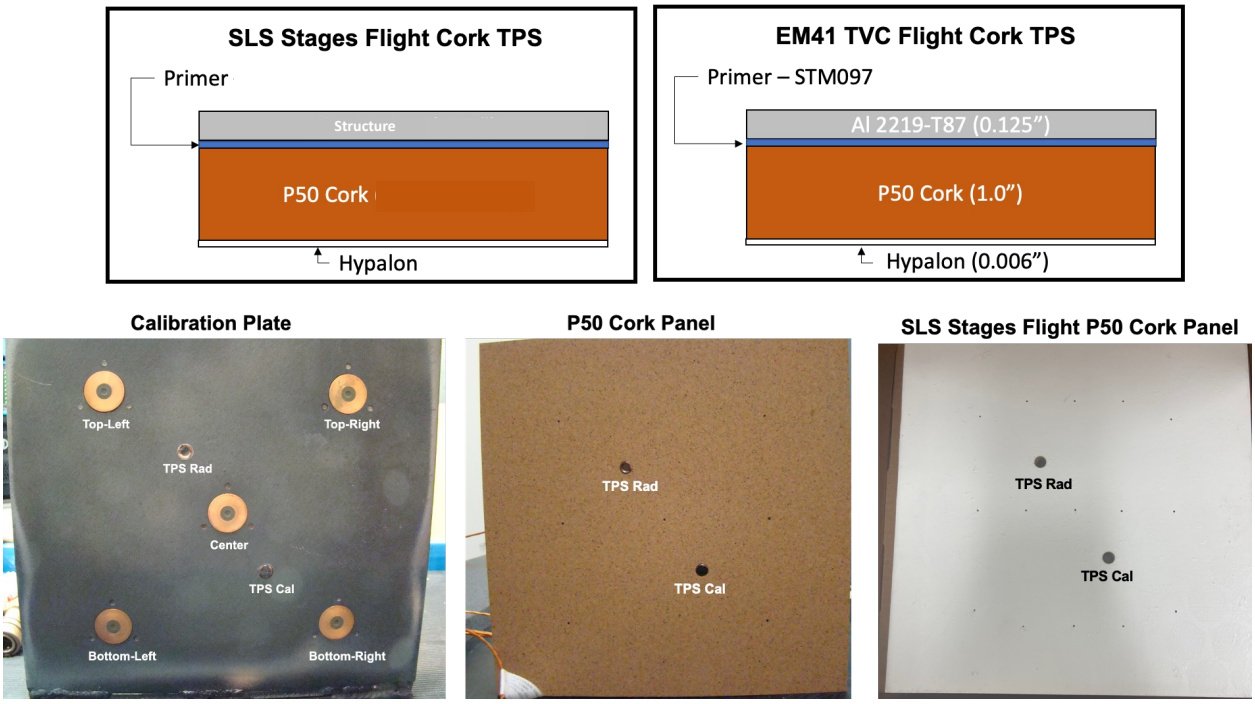

Figure 9. Comparisons of the TVC radiative heating TPS sample stack-up and the generalized SLS Core Stage base heat shield TPS stack-up (top); TVC calibration plate (bottom left), P50 cork panel (bottom middle) and Hypalon coated P50 cork panel (bottom right).

Figure 10 shows the various regions on the SLS Core Stage which contained Hypalon-coated P50 cork as the TPS. The largest acreage of this TPS was on the base heat shield and boattail which are both components encompassing the base region of the Core Stage. It was also found extensively on the barrel engine section and intertank. P50 cork is being planned as the most widely used ablator TPS on SLS for many of the high thermal environment areas for Artemis II through Artemis V. Cork is also used as an ablator TPS on other elements of the SLS and Orion vehicles such as the solid rocket boosters and the launch abort system (LAS).

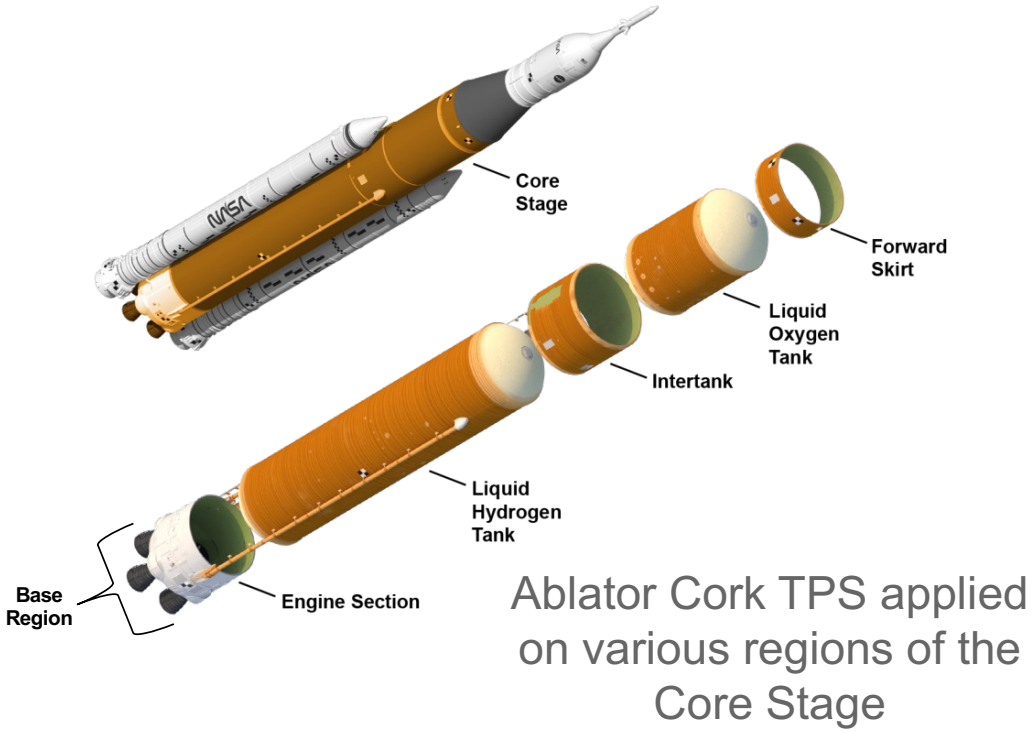

Figure 10. SLS Core Stage layout.

Table 1 shows the test matrix for the TVC P50 cork radiant heating and response characterization test campaign. This test campaign varied the total heating (radiant heating) from 4 BFS to 12 BFS and the ambient pressure varied from sea-level to 1.9 psia. Initial radiant and total heating rates were representative of a typical launch vehicle ascent environment. Air and nitrogen were used as the ambient medium in the TVC. Two TPS samples were used: (1) Hypalon-coated P50 cork and (2) non-coated P50 cork. This test operation was an innovative approach in modifying the facility to gather important ground test data in support of Green Run and Artemis 1 flight data. It was the first test within TVC that provided in-situ TPS measurements of the cork combustion phenomena while simulating launch vehicle ascent conditions. All tests were conducted at similar test durations. APP refers to simultaneously reducing the TVC ambient pressure, similar to a launch vehicle ascent profile, during TPS testing. Variation in the air mass flow rate over the TPS panel was also done, as shown in Table 1, by varying the air input pressure to simulate air entrainment over the SLS Core Stage base heat shield. All of the TPS samples were subjected to a constant radiative heating source and ambient pressure, but 8 tests varied the ambient pressure as a function of time. The test matrix also includes which post-test specimens were sectioned to intrusively measure the recession, char layer, and pyrolysis layer or were delivered for X-Ray CT scanning to obtain these measurements, non-intrusively.

Air inlet pressure tests were conducted in the TVC to estimate the mass flow rate being introduced over the TPS panel. Three pressure set points were supplied to the sealed TVC at sea-level conditions. A few sub-atmospheric pressure points and the rise in the TVC ambient conditions as a function of time were recorded. Air mass flow rate can be theoretically calculated from Equation 1 using (1) the ambient pressure and temperature rise slope, dP/dt and dT/dt, (2) the ambient temperature (T), ambient pressure (P) and volume of the TVC (V) and (3) air gas constant (R). All these measurements were provided at 3 pressure inlet set points, 20, 40, and 80 psig which translated to air mass flow rates of 0.007, 0.013, and 0.025 lb_m/sec that passes over the TPS surface panel, respectively. These values were based on taking a mean from the various runs at a set jet initial pressure.

$$\dot{m}_{air} = \frac{V}{R}\left[\frac{1}{T(t)}\frac{\partial P}{\partial t} - \frac{P(t)}{T(t)^2}\frac{\partial T}{\partial t}\right] \quad (1)$$

Table 1. TVC radiative heating test matrix.

Test Run	Heat Rate (BFS)	Ambient Pressure (psia)	Air Input Pressure (psig)	Sample	Test Gas	Section/HG F/Xray CT	Specimen Number	Ascent Press Profile (APP)	Comments
042	7.6	Varies	0	P50 Cork	Air	Section	1699B-01	APP 1	Smoke, Flamelet
058	7.6	14.7	0	P50 Cork	Air	Section	1699B-06	N/A	Smoke, Flamelet, Pyrolytic gas burning?
060	7.6	7.8	0	P50 Cork	Air	Section	1699B-08	N/A	Smoke, Flamelet, Pyrolytic gas burning?
063	7.6	Varies	0	P50 Cork	Air	Section	1699B-10	APP 2	Smoke, Flamelet, Pyrolytic gas burning?
065	7.6	3.9	0	P50 Cork	Air	Section	1699B-12	N/A	Smoke
067	7.6	14.7	0	P50 Cork	N2	Section	1699B-03	N/A	Smoke, Flamelet, Pyrolytic gas burning?
069	7.6	14.7	80	P50 Cork	Air	X-Ray CT HGF	1669B-07	N/A	Simulate base air flow, Smoke, Flamelet, Large-Scale Fire
072	7.6	7.8	80	P50 Cork	Air	X-Ray CT HGF	1699B-09	N/A	Simulate base air flow, Smoke, Flamelet, Large-Scale Fire
074	7.6	1.9	0	P50 Cork	Air	X-Ray CT HGF	1699B-13	N/A	Obtain minimal O2 availability, Smoke
078	7.6	Varies	80	P50 Cork	Air	X-Ray CT HGF	1699B-02	APP 3	Simulates base air flow, Smoke, Flamelet, Large-Scale Fire, Pyrolytic gas burning?
082	3.8	Varies	80	P50 Cork	Air	RTC	1699B-05	APP 3	Simulates base air flow, Smoke
084	3.8	14.7	80	P50 Cork	Air	RTC	1699B-04	N/A	Simulates base air flow, Smoke
089	**7.6**	**Varies**	**80**	**Hypalon/P50 Cork**	**Air**	X-Ray CT HGF	**1699B-21**	**APP 3**	**Flight Case 1, Simulates base air flow, Smoke, Flamelet, Large-Scale Fire, Pyrolytic gas burning?**
100	7.6	Varies	40	P50 Cork	Air	X-Ray CT HGF	1699B-11	APP 3	Effect of base air flow rate, Smoke, Flamelet, Large-Scale Fire, Pyrolytic gas burning
102	**7.6**	**14.7**	**40**	**Hypalon/P50 Cork**	**Air**	X-Ray CT HGF	**1699B-20**	**N/A**	**GR HF Case 1, Simulates base air flow, Smoke, Flamelet, Large-Scale Fire, Pyrolytic gas burning**
109	11.5	Varies	40	P50 Cork	Air	X-Ray CT HGF	1699B-14	APP 3	Effect of higher heating rate, Smoke, Flamelet, Large-Scale Fire, Pyrolytic gas burning
097	**11.5**	**Varies**	**80**	**Hypalon/P50 Cork**	**Air**	X-Ray CT HGF	**1699B-22**	**APP 3**	**Flight Case 2, Simulates base air flow, Smoke, Flamelet, Large-Scale Fire, Pyrolytic gas burning**
104	7.6	Varies	20	P50 Cork	Air	RTC	1699B-15	N/A	Lower inlet pressure, Smoke, Flamelet

III. Results

A. Time Evolution Imagery Data Sets

The high-definition (HD) visible video camera was positioned orthogonal to the area between the TPS panel and radiative quartz lamp. In the Figures 11 – 14, the radiative lamp is to the right of each image and is not observed. The TPS panel and the associated fixtures are visible to the left within each image. Figure 11 shows time evolution images of the TPS and environment response for Run 82, the lowest radiative heating input with an ascent profile and high air entrainment. Note that the radiant heat lamps were activated at T+0 seconds in all the test runs. At T+22 sec, significant TPS outgassing and smoke was observed above the P50 cork panel. Since the TVC was a closed volume chamber and the rate of outgassing exceeded the rate of vacuum pumping, the optical depth of the smoke significantly increased by T+44 sec and the panel could no longer be seen, after which the test panel was obscured until tests terminated at T+140 seconds.

Figure 12 shows the time evolution images for Run 42, the nominal radiative input heating at 7.6 BFS with an ascent profile and no forced air. Each image in Figure 12 had a lower ambient pressure than the preceding image. At T+12 and T+18 seconds, smoke and outgassing were observed emanating from the TPS panel. This was seen as white wisps of smoke near the trailing edge of the TPS panel. Between T+26 sec to T+44 sec, small flamelets with smoke

was observed at the leading edge of the panel and near the corners. From visible imagery alone it was difficult to confirm if there was a poorly established flame front and/or smoke. There was some structure in the flow above the TPS panel and a tinge of orange hue, indicating a weak flame front with excessive smoke above the panel. It was seen that this flow structure starts at the leading edge and propagates to the trailing edge, where there was significant turbulence observed. Beyond T+55 sec, the main feature from the imagery video was dominated by smoke with no evidence of a poorly established flame. Although not shown here, the test with nitrogen gas did not show characteristic cork combustion phenomena, but rather extensive smoke emanating from the panel, similar to Run 42.

Figure 13 shows the time evolution images for Run 97, the nominal radiative input heating with an ascent profile and forced air. Between T+10 to T+15 seconds, uniform outgassing and smoke was observed above the TPS panel. At T+18 seconds, a strong dark orange flame front was first seen established at the leading edge of the panel. There seemed to be a larger prevalence of smoke near the trailing edge of the panel. From T+15 sec to T+81 sec, the flames were attached to the cork TPS and after T+45 seconds, strong turbulent flames were observed attached above the TPS panel (noted as “attached flames”). At T+112 seconds as the ambient pressure was below a threshold, the flames detached from the TPS panel, and the flames were observed in the freestream (noted at “detached flames”). Above T+112 seconds, the intensity of the flames in the freestream decreased as the ambient pressure decreased and no evidence of smoke was observed adjacent to the cork panel. Beyond T+112 sec, the Hypalon paint can be observed charred and peeling from the P50 cork substructure. Figure 14 shows the time evolution images for Run 100, nominal radiative input heating with an ascent profile and forced air. A similar flow field and flame structure was observed between Run 97 and Run 100, but the only difference was that Run 100 had bare P50 cork as the TPS sample. Large-scale attached turbulent flames were observed from T+27 sec to T+92 sec. Above T+100 sec, detached flames were observed and propagated within the freestream, similar to Run 97. Although only two time-evolution imagery data of the cork combustion dynamics are shown in this paper, all test runs where cork combustion was observed show very similar findings in the dynamics such as initial heating, ignition, flame propagation and detached flame characteristics. Eight out of the 18 test panels showed similar large-scale TPS fire and cork combustion dynamics.

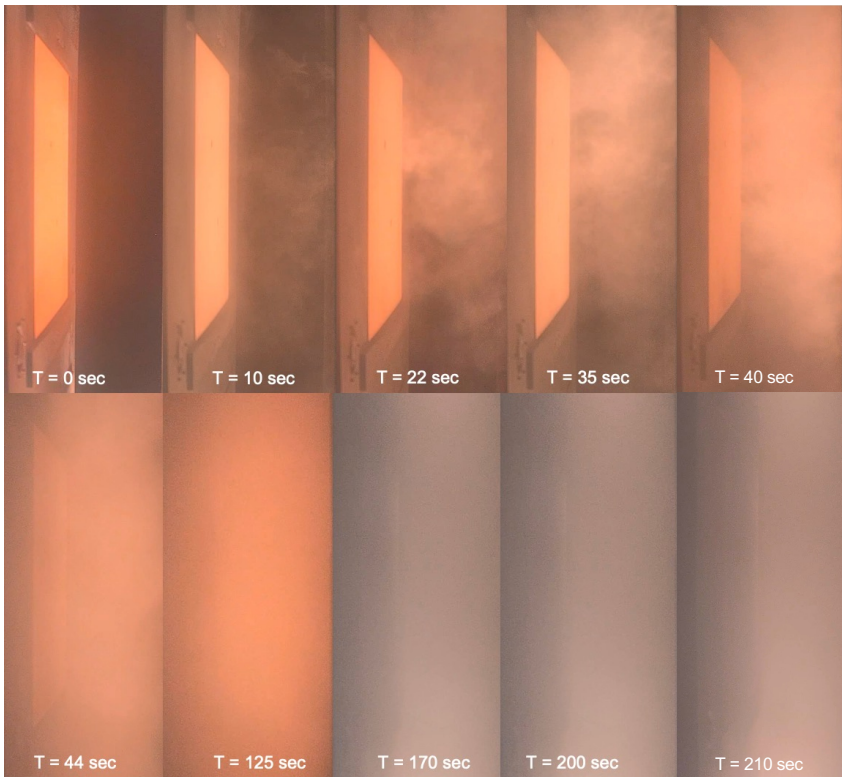

Figure 11. Visible imagery time evolution of Run 82.

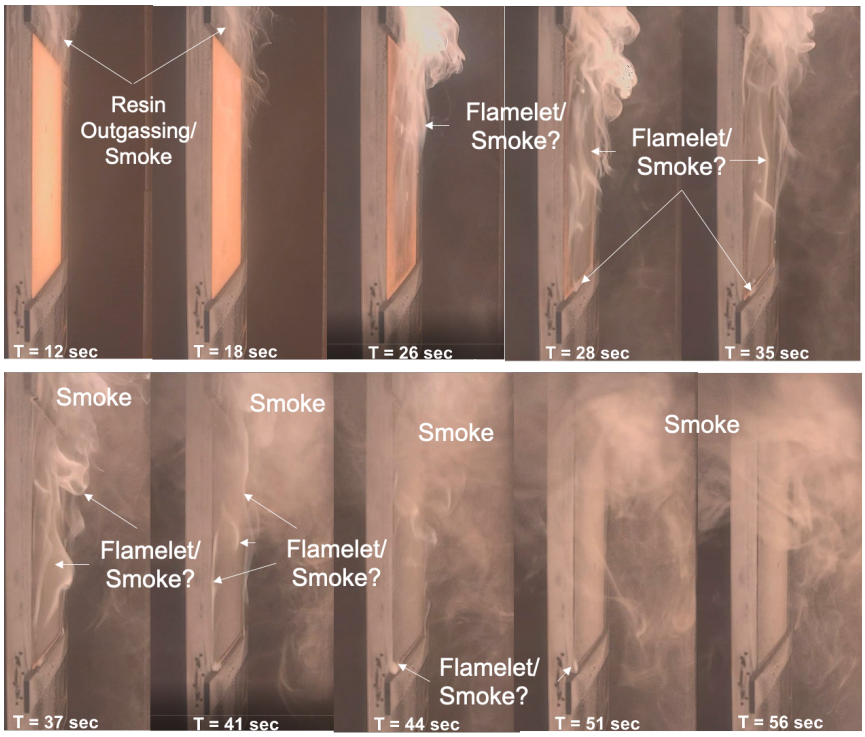

Figure 12. Visible imagery time evolution of Run 42.

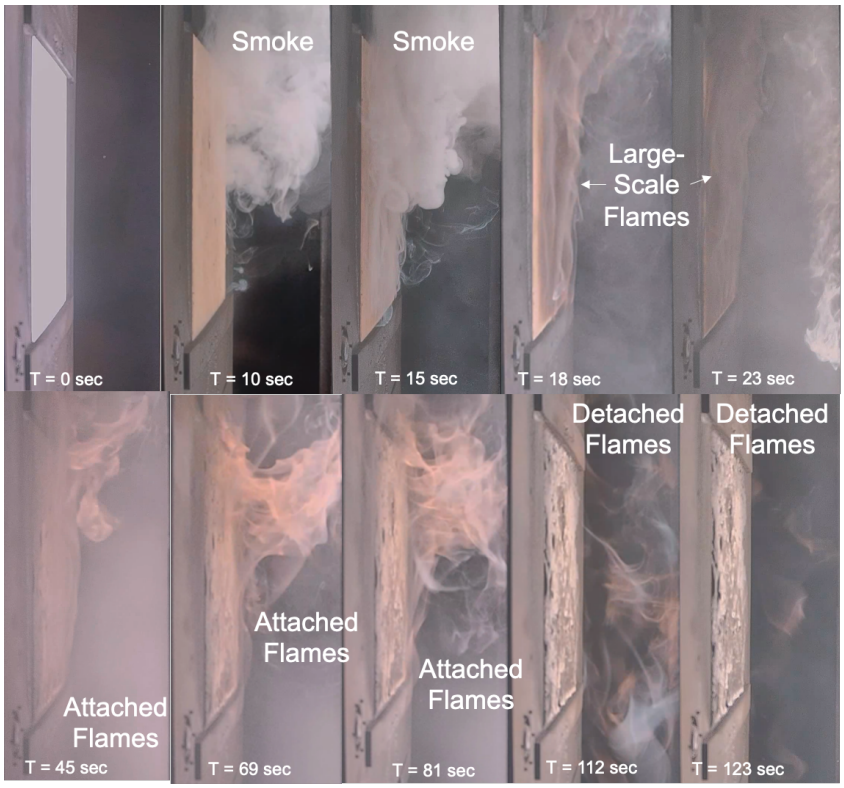

Figure 13. Visible imagery time evolution of Run 97.

Figure 14. Visible imagery time evolution of Run 100.

B. Test Instrumentation Data Sets

Figures 15–19 display measurements from the embedded, co-located TPS calorimeter and radiometer, which were flush with the surface of the P50 cork panel. These measurements, taken over the full duration of the test, represented the first such data collected within the TVC. Figure 15 corresponds to Run 82, which involved low radiative heating input, an ascent profile, and forced air. The left panel shows the distributions of radiative heating (blue curve), total heating (red curve), and ambient pressure (green curve) as a function of test time. High-definition visible images are also included to correlate with the heating distributions. The two smaller panels on the right illustrate the convective heating rates as a function of ambient pressure and test duration. The black curve represents the raw hot-wall convective heat flux distribution. Occasionally, two black curves are present in the heat flux vs. ambient pressure plots, which occurs when ambient pressure rises following the shutdown of the radiant lamps at T+110 seconds. The red curve represents the corrected hot-wall convective heating distribution, while the green curve shows the cold-wall convective heat flux distribution. It is important to note that the cold-wall convective heat flux during the TVC test was estimated based on the assumption that the TPS burning gas recovery temperatures were similar to those observed in the Green Run, which analyzed base heat shield cork combustion dynamics. Additionally, the corrected convective heating remained below 1 BFS for the entire duration of Run 82, which was supported by the lack of visible observation of a flame front. For the radiative heating, corrections were made to account for potential soot buildup on the gauge and/or significant optical depth of smoke, both of which could attenuate radiation. This correction aligned with the imagery data, which showed no evidence of cork combustion during the test.

Figure 16 presents embedded TPS measurements for Run 42, where the convective heating increased to just under 2 BFS. This suggests that heat release occurred during the outgassing or minor smoldering of the P50 cork at the ignition point, which occurred at T+25 seconds. The smoldering persisted throughout the test duration, continuing until the shutdown of the radiative lamps. In Run 67, which used N_2 test gas, there was a modest increase in convective heating, likely due to the generation of pyrolytic gases and TPS thermal degradation. The heating distributions observed in Run 67 were similar to those in Run 42.

Figures 17 through 19 illustrate the typical combustion phenomena of P50 cork. At the cork ignition point, a significant, discontinuous increase in both total and convective heating rates occurred between T+15 and T+25 seconds. During this period, convective heating rose sharply by 4 to 5 BFS, followed by a modest decline until the system reached a quasi-steady state burning environment. Once the radiant quartz lamps were turned off, the convective heating rate dropped dramatically, nearing 0 BFS. This indicated that cork combustion was not self-sustaining and required an external heat source to elevate the TPS surface temperature above the ignition threshold. The radiative heating environment substantially decreased during the cork combustion process for two primary reasons: (1) significant radiation attenuation due to smoke and TPS out-gassing, and (2) soot accumulation on the radiometer window, which further blocked incoming radiation. It was challenging to determine which of these factors played a dominant role in the reduction of radiative heating in each test run. However, it was hypothesized that the sharp decrease in radiative heat flux measurements during large-scale TPS burning was due to sensor contamination by soot. This situation highlighted the need for radiative heating corrections to properly assess the convective heating distributions. The abrupt decline in radiative heating was inconsistent with observations from the Shuttle and Artemis I flights, where soot was significantly entrained due to vehicle acceleration. In contrast, the radiative heating measurements in the TVC tests, during the quasi-steady cork burning phase, were below 2 BFS. Similar environment observations were noted during the Green Run test program and the Artemis I flight, particularly on the instrumentation of the base heat shield[1-2,5]. In fact, 8 out of 18 test runs exhibited high convective heating and low radiative heating, attributable to the P50 cork combustion dynamics and large-scale burning along the TPS panel. Most of these test runs required a radiative heating input threshold exceeding 6 BFS and forced air to sustain large-scale burning. Figures 17 to 19 also show a slight decrease in total and convective heating near T+100 seconds, corresponding to changes in cork combustion dynamics, as discussed in Section IV, Discussion and Analysis.

The embedded TPS and TVC chamber instrumentation demonstrated strong alignment with video imagery data sets, providing an effective assessment of these complex two-way coupled environments. This marked the first detailed investigation into the interaction between the TPS and gas environment, although similar phenomena had been observed in earlier TVC P50 cork test campaigns. Prior to the Green Run, most studies focused exclusively on one-way coupled gas-phase plume environments[3,7]. It was previously believed that the high-enthalpy gas in one-way coupled conditions was responsible for the convective heating on the base heat shield. These observations, along with the study of large-scale TPS burning observed during Green Run and Artemis I flight[1-2,5], have led to a closer integration of the fields of aerothermodynamics and thermal protection systems (TPS).

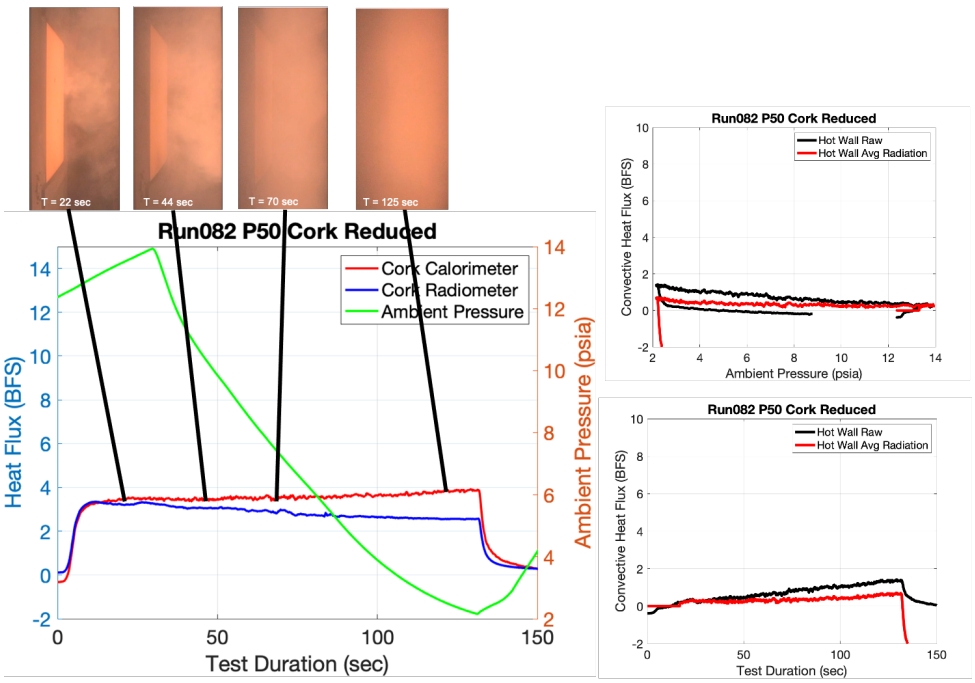

Figure 15. Run 82: (left) embedded TPS heat flux and ambient pressure vs. time; (top-right) embedded TPS convective heat flux vs. ambient pressure; (bottom-right) embedded TPS convective heat flux vs. time.

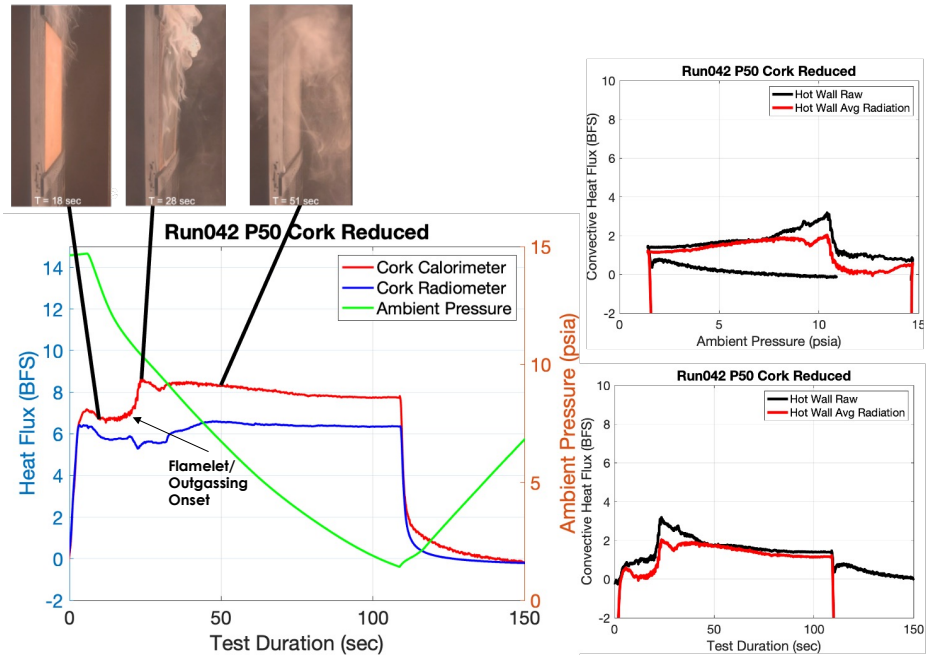

Figure 16. Run 42: (left) embedded TPS heat flux and ambient pressure vs. time; (top-right) embedded TPS convective heat flux vs. ambient pressure; (bottom-right) embedded TPS convective heat flux vs. time.

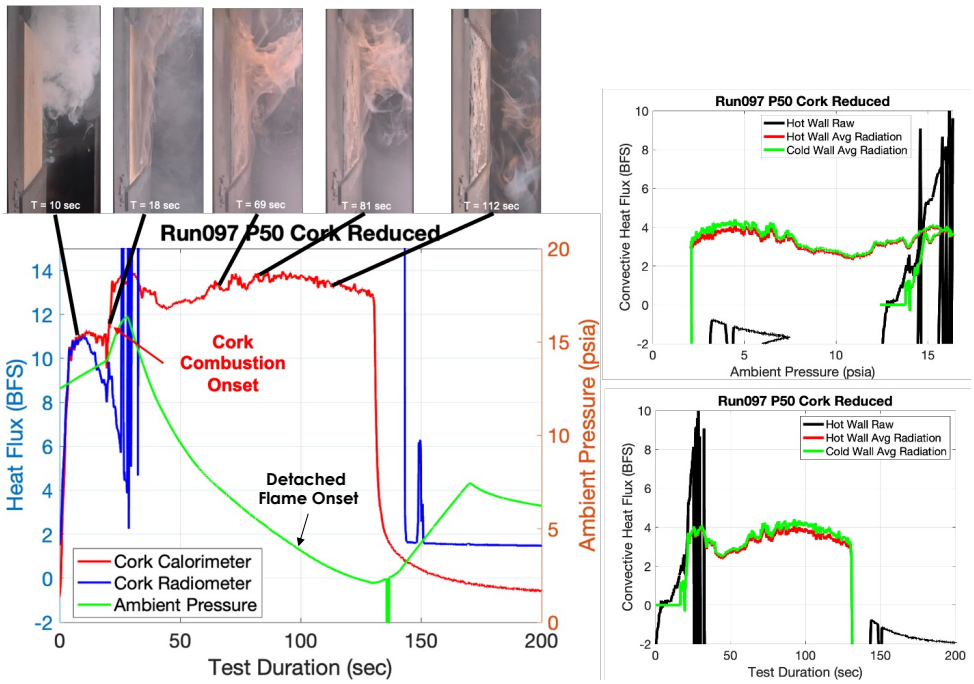

Figure 17. Run 97: (left) embedded TPS heat flux and ambient pressure vs. time; (top-right) embedded TPS convective heat flux vs. ambient pressure; (bottom-right) embedded TPS convective heat flux vs. time.

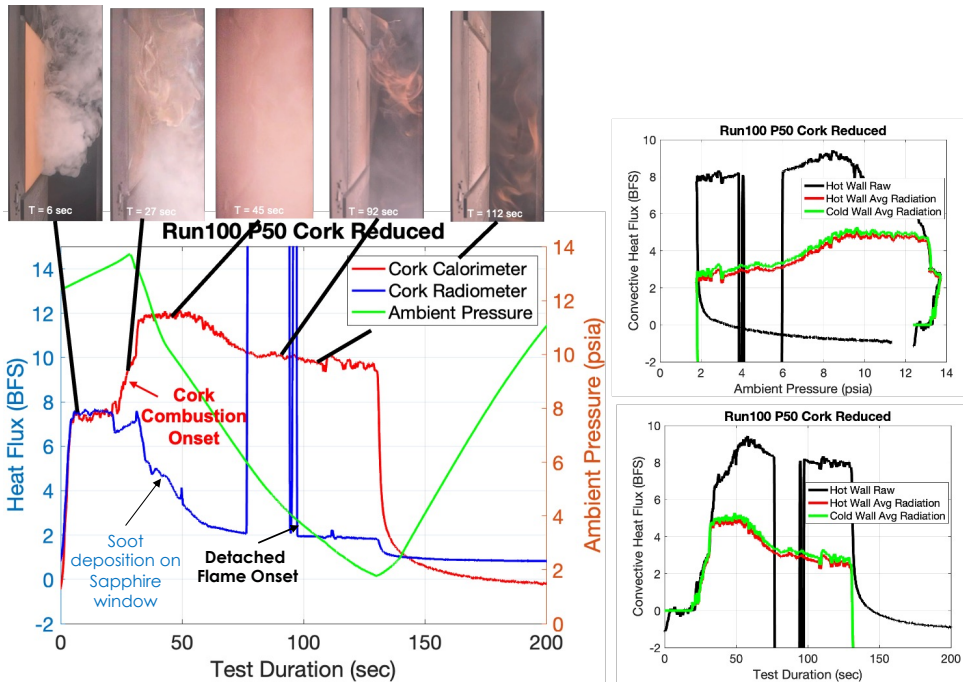

Figure 18. Run 100: (left) embedded TPS heat flux and ambient pressure vs. time; (top-right) embedded TPS convective heat flux vs. ambient pressure; (bottom-right) embedded TPS convective heat flux vs. time.

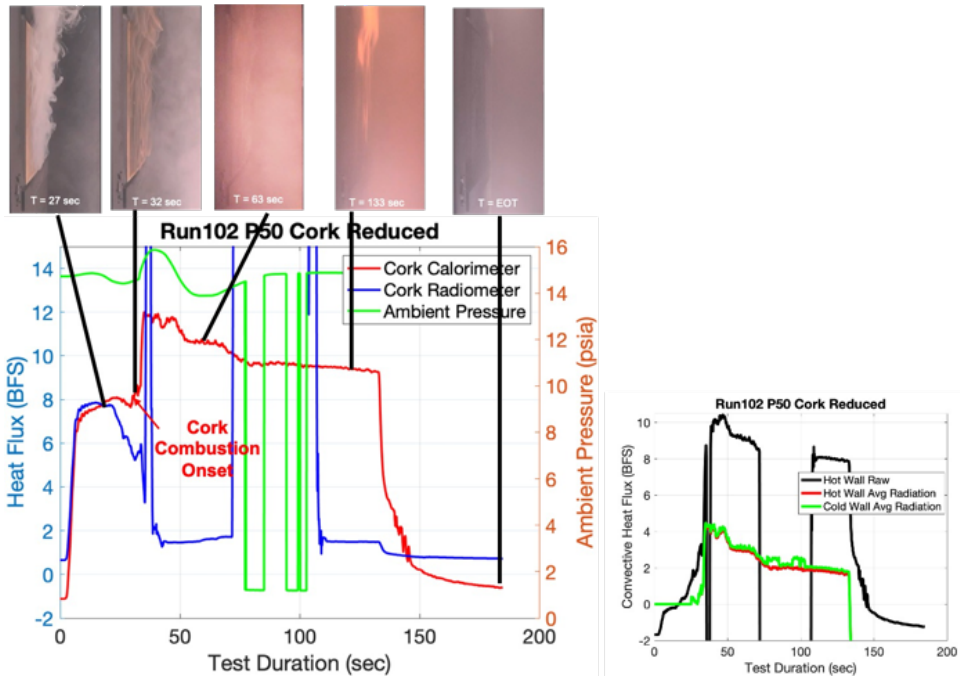

Figure 19. Run 102: (left) embedded TPS heat flux and ambient pressure vs. time; (top-right) embedded TPS convective heat flux vs. ambient pressure; (bottom-right) embedded TPS convective heat flux vs. time.

C. Pre-TVC and Post-TVC TPS Panel Imagery Data

Figures 20 – 24 show still images of the side and top-down view of the TPS panels prior (left) and post-TVC (right) testing. Blue arrow shows the direction of the forced air flow along the TPS panel. There were two holes in the

TPS panel which was where the embedded calorimeter and radiometer instruments were located. Figure 20 shows the TPS response of minimal radiative heating and with no cork combustion phenomena. Minimal deep charring was observed on this panel and only surficial char can be observed. Forced air flow for this test run as shown in Figure 20 leads to convective cooling and reduces surface total heating which led to minimal surficial charring in that region of the panel. Higher radiative heating was observed on the left region of the panel where air flow was minimized, and more surficial charring was observed. Figure 21 shows a test sample where there is nominal radiative heating, but no air entrainment introduced over the panel. This leads to an alligator-skin surface topology appearance characteristic of radiative and convective heating with minimal shear stress.

Figures 22-24 show images of TPS panels after a cork combustion burning process for over 50 seconds. This led to a much more extensive deep charring and a darker surface char. There was a honeycomb surface layer look on the top of the TPS, similar to an arid crust sand layer within a desert region. This observation was also noted from a radiative heating-only environment. Figures 22 and 24 shows portions of the Hypalon paint burned away exposing the significantly charred P50 cork during the combustion process.

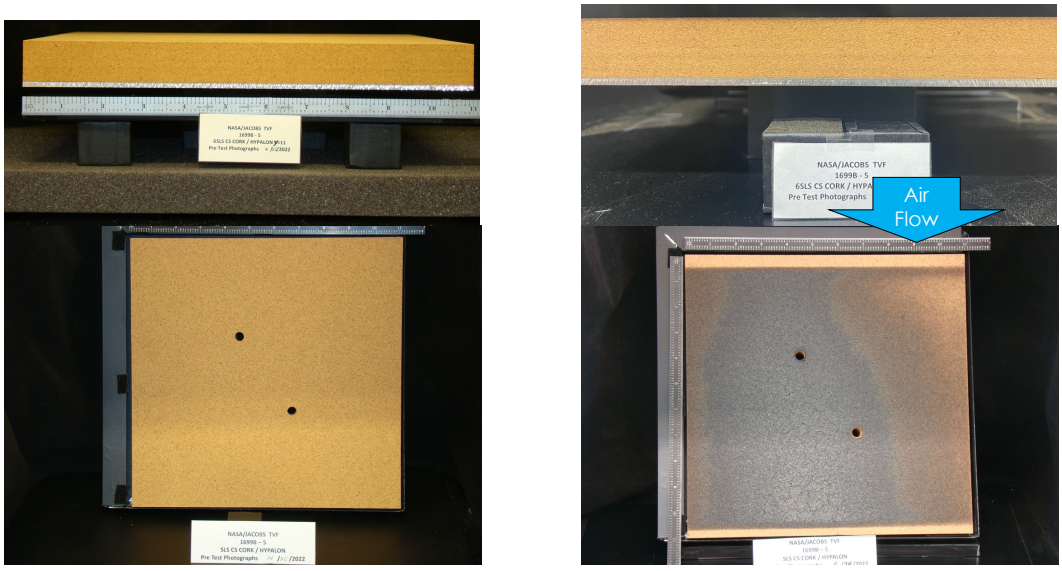

Figure 20. Run 82: (top-left) side and (bottom-left) top-down views of pre-TVC test TPS panel; (top-right) side and (bottom-right) top-down views of post-TVC test TPS panel.

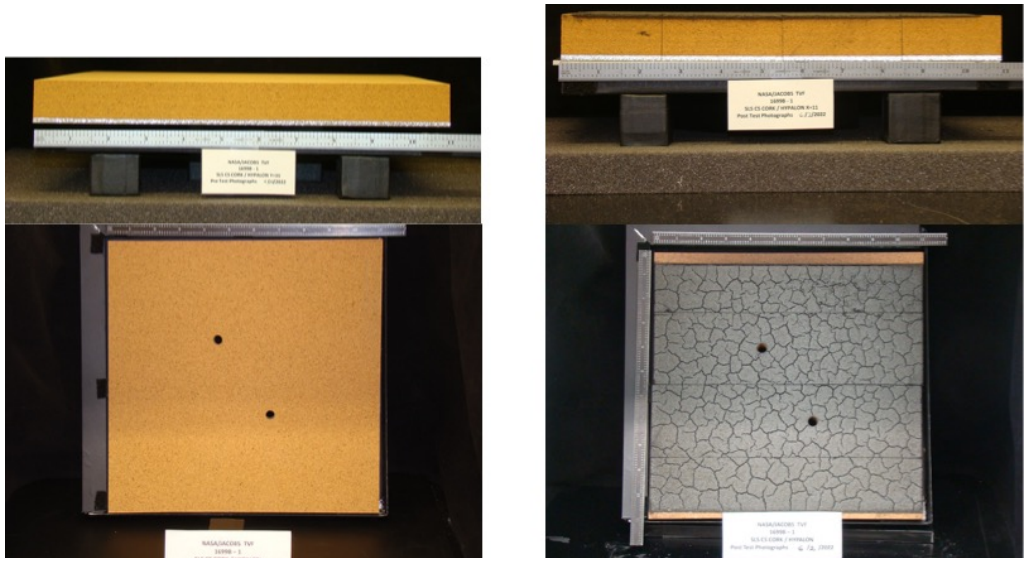

Figure 21. Run 42: (top-left) side and (bottom-left) top-down views of pre-TVC test TPS panel; (top-right) side and (bottom-right) top-down views of post-TVC test TPS panel.

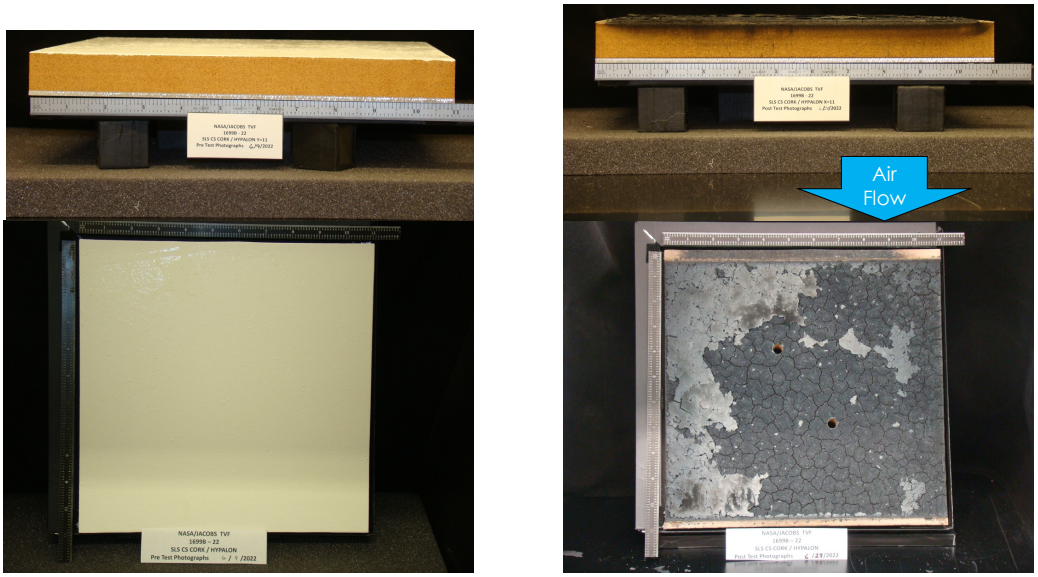

Figure 22. Run 97: (top-left) side and (bottom-left) top-down views of pre-TVC test TPS panel; (top-right) side and (bottom-right) top-down views of post-TVC test TPS panel.

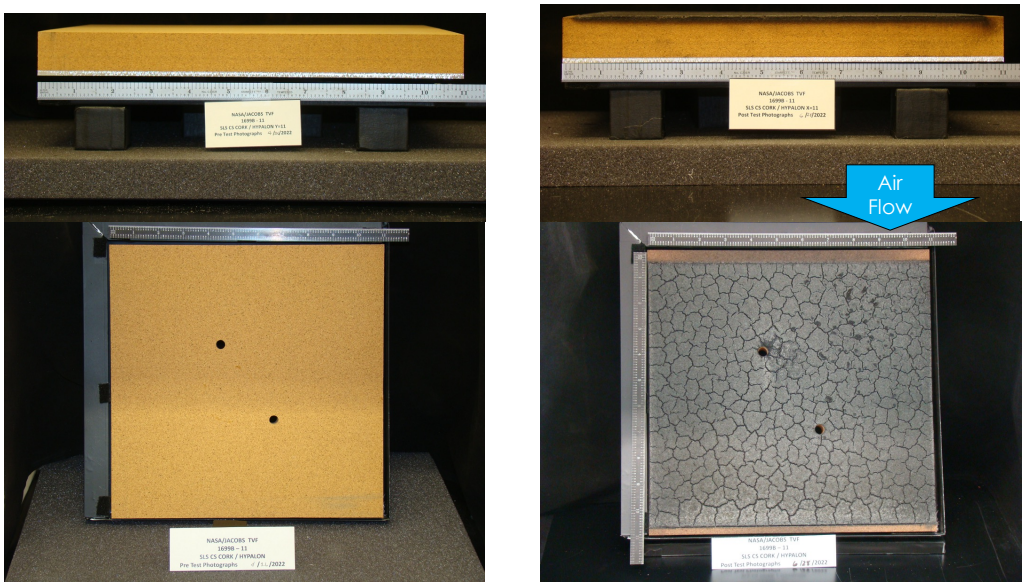

Figure 23. Run 100: (top-left) side and (bottom-left) top-down views of pre-TVC test TPS panel; (top-right) side and (bottom-right) top-down views of post-TVC test TPS panel.

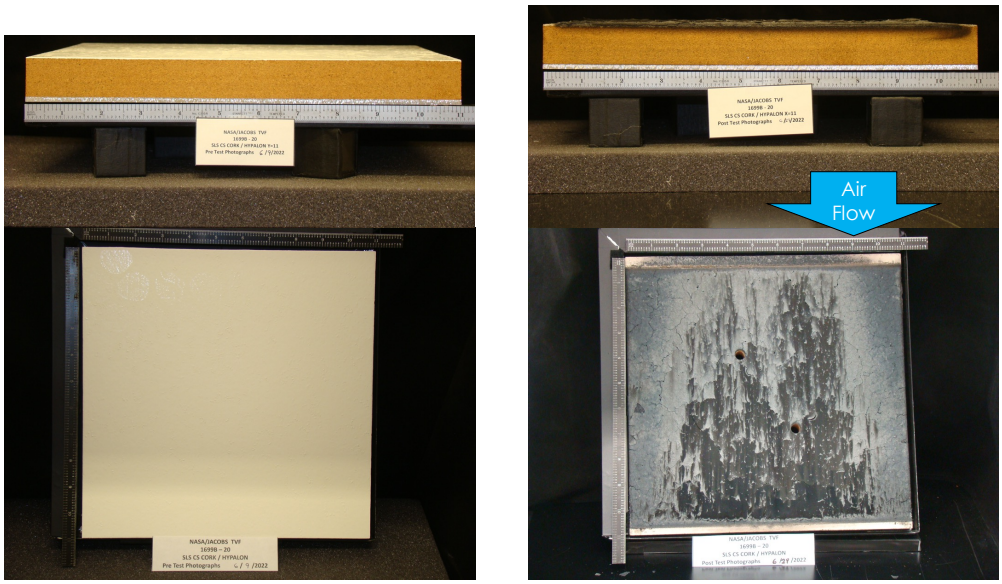

Figure 24. Run 102: (top-left) side and (bottom-left) top-down views of pre-TVC test TPS panel; (top-right) side and (bottom-right) top-down views of post-TVC test TPS panel.

D. X-Ray CT Scans of the Post-TVC TPS Panels

X-Ray Computed Tomography (CT) was completed for the full 3-D TPS specimen of a subset of post-TVC tests. Figures 25 – 28 show a cross-section CT image that bisects a region where flight instrumentation was embedded. Darkest intensity was representative of air density and the lightest intensity was closer to the densest P50 cork virgin material. Figure 25 for Run 97, the high density Hypalon paint was seen above the P50 cork sub-surface TPS. Figure 26 shows a sharp intensity gradient in the char layer which suggested a much lower density char layer than Run 97. There was X-Ray CT artifact where the aluminum substrate was reflecting X-ray which diffuses into the virgin P50 cork layer. Figure 27 shows another sharp intensity gradient between the P50 cork char layer and virgin material suggested a low-density char layer. It also showed the high density Hypalon paint partially attached to the P50 cork TPS.

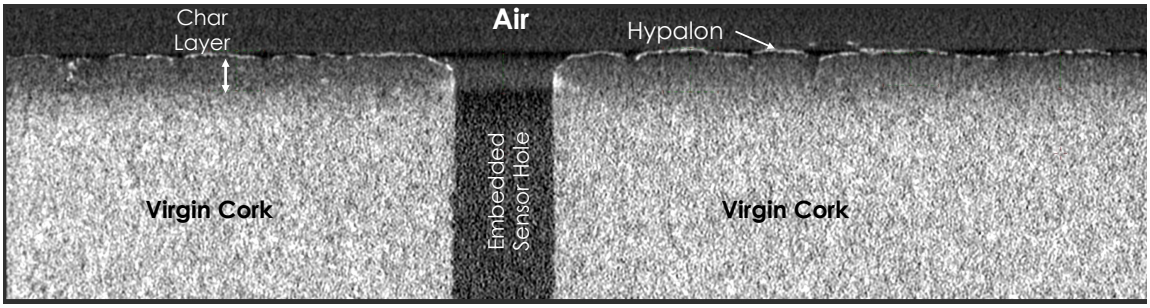

Figure 25. Run 97: X-Ray CT scan thru a section of a post-TVC test TPS panel.

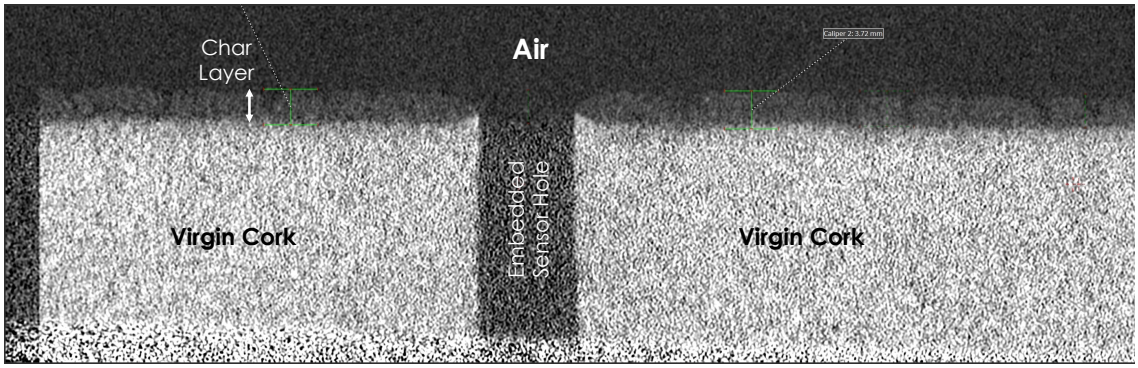

Figure 26. Run 100: X-Ray CT scan thru a section of a post-TVC test TPS panel.

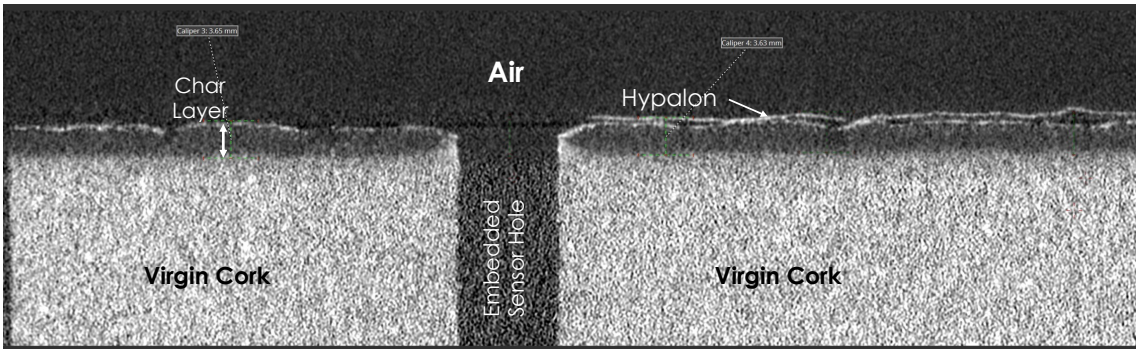

Figure 27. Run 102: X-Ray CT scan thru a section of a post-TVC test TPS panel.

IV. Discussion and Analysis

Figure 28 shows a comparison of the calorimeter measurements within the P50 cork surface between the TVC and Green Run hot-fire testing[2]. It was seen that that P50 cork combustion heating trends were similar between the TVC ground test and flight-scale test. It should be noted that the green curve on the left of Figure 28 shows the ambient pressure within the TVC which is on the order of sea-level and the green curve on the right of Figure 28 is the RS-25 combustion chamber pressure which operated at sea-level pressure. Much higher frequency data was available during the Green Run test[5] than the TVC test which led to higher scatter in the total heating rates (red curve) during the cork combustion regime. The total, convective and radiative heating rate distributions showed similar trends during the cork combustion phenomena between the TVC at sea-level ambient pressures and Green Run static test campaigns[5]. There was a large jump in total heating (convective heating) and a steep reduction in radiative heating at the ignition point. Both data sets followed with a slight decrease in the total heating but a quasi-steady burning environment. Both data sets showed imagery of large-scale deflagration of the cork TPS. These two data sets confirmed that the Green Run base heat shield environments were not an artifact of the static ground test configuration or scale. However, the absolute heating rate magnitudes between test and flight were not similar.

Figure 29 shows the peak convective heating rate and mean convective heating rate distribution with respect to mean input radiative heating rates imparted onto the P50 cork panel by the radiative lamps. There were three general categories of observations noted from the visible imagery video data sets: (1) cork combustion which includes well-established attached turbulent flames on the TPS; (2) smoke/flamelet where a not-well established flame front clouded with excessive smoke; (3) smoke and outgassing. It was seen that the highest convective heating environment occurs during the cork combustion regime which led to the maximum exothermic release of energy from P50 cork char oxidation and pyrolytic gas – air reactions and where smoke/outgassing led to a much-reduced energy release[5,9,10]. Char oxidation led to a significant energy release[9,10]. Cork combustion was observed for all TVC cases where the radiative heating imparted to the panel was greater than 6 BFS in the presence of forced entrained air. When forced air entrainment was not imparted on the TPS panel, the lack of mass flow rate and well-mixing of air with the pyrolytic gases was not established, leading to a much-reduced heat release, poorly formed flamelets and extensive smoke.

Although not observed in the TVC test program, cork combustion was observed during Green Run for initial pre-burning total heating of 3 BFS and higher which may be a function of the higher entrained air mass flow rate.

The chemical composition of P50 cork material was about 27% lignin, 45% suberin, 12% polysaccharides 6% ceroids and 6% tannins[8]. P50 cork (phenolic resin cork with 50 um granule diameter) ablator was developed by the Amorim Corporation. All these chemicals contained C, H, and O molecules. These hydrocarbons contain a high molar mass of carbon[9,10]. As shown in Equations 2 and 3, solid *(s)* P50 cork char carbon ($\dot{m}_{char}$) oxidizes with oxygen from air ($\dot{m}_{air}$) leading to highly exothermic reactions and the formation of carbon monoxide and carbon dioxide gases (Figure 30)[7,8]. The solid char on the TPS surface was seen in the post-TVC test images as the blackened material (Figure 17). These exothermic reactions due to char oxidation of the material released light and induced high thermal energy[7] *(+*$Q_{release}$) in the form of a discontinuous increase in gas recovery temperature (T_g), leading to an increase in convective heating ($\dot{q}_c$) to the TPS surface. These variables of the cork combustion process are depicted in the schematic shown in Figure 30. The sudden increase in the gas recovery temperature due to P50 cork ignition and combustion was not measured within these TVC test programs due to a lack of MEDTHERM GTP measurements on the surface of the TPS[8], but such measurements were recorded on the Core Stage base heat shield during the Green Run test program, and Artemis I flight. However, the ambient gas temperature towards the back of the TPS panel for the TVC test program did observe an increase due to cork combustion processes as shown in Figure 35. Only qualitative trends were used for assessment.

Another important component of the exothermic reaction was the reactions of pyrolytic gases with air. These gases were seen emanating from the TPS surface in Figure 11 to Figure 14. Pyrolysis is the chemical degradation process which is enabled by high temperature in the presence of an inert atmosphere. Pyrolysis can produce solids (char), condensable liquids (oils and tar) and non-condensable gasses. Pyrolytic zone, where pyrolysis is actively occurring in a TPS layer, was observed between the char layer and the virgin P50 cork layer[9,10]. The pyrolysis process produced gas which increases the pore pressure within the TPS. This gradient in pressure between the pyrolytic zone and the freestream air led to movement of the pyrolytic gases to escape through the TPS surface. This then led to burning of the pyrolytic gases ($\dot{m}_{pyro}$) with oxygen from air, high gas recovery temperatures and high TPS surface temperatures (Figure 30). Unlike the processes of char oxidation, pyrolytic gas oxidation is more difficult to accurately assess due to the multitude of pyrolytic gases that are emanating from the pyrolysis layer within the TPS to the freestream. P50 cork and its binder material, Quercus Suber phenolic resin, led to the generation of these combustible gases. Pyrolytic gases were generated at temperatures between 851 deg R and 1267 deg R and thermogravimetric analysis (TGA) results suggested that the ablation temperature of cork was at 920 deg R[5,9,10]. Based on TVC tests, pyrolytic gases started emanating from the TPS surface at about T+10 seconds.

$$C(s) + \frac{1}{2}O_2 \rightarrow CO \;\; \Delta H_{RXN} = -110.5\, BTU/mol \quad (2)$$

$$C(s) + \; O_2 \rightarrow CO_2 \;\; \Delta H_{RXN} = -372.9\, BTU/mol \quad (3)$$

Figure 31 shows the mean convective heating rate as a function of both the ambient pressure and the entrained air mass flow rate. It was seen that as the oxygen availability or concentration decreases this leads to a reduction in convective heating due to cork combustion. Forced entrained air led to a larger amount of oxygen concentration and more effective mixing with the pyrolytic gases, enhancing the combustion temperature and convective heating due to cork combustion. Figure 31 shows that as the forced entrained mass flow rate increases, increasing the local oxygen concentration, this led to an increase in the convective heating due to cork burning. The TVC was limited to the amount of air flow rate and during launch vehicle ascent the entrained air flow can be substantially higher due to vehicle speeds above Mach 1. This could result in higher combustion temperature and higher convective heating due to cork burning than what the TVC test program produced. Such observation was noted during Artemis I flight[1].

One of the main objectives of the TVC test program was to determine when P50 cork combustion would cease due to lack of oxygen concentration as the launch vehicle ascends into the atmosphere. Although we did not measure oxygen concentration in this test, ambient pressure was measured. Figure 32 shows convective heat rate reduction factor at the detached flame onset as a function of ambient pressure. It was observed that the detached flame onset occurred at an average ambient pressure of 3.5 psia which correlates to an altitude of about ~38,000 ft. This occurs at a flight time of T+ 65 sec. The detached flame regime within the ground test generally occurred at T+100 sec for all large-scale cork burning panels (Figures 17-19). Detached flame led to a reduction in cork combustion convective

heating rates and combustion temperature since the flame has a stand-off distance from the TPS surface. This stand-off distance increases with a reduction in ambient pressure and reduces the local gas temperature near the cork surface. The theory is that as the pyrolytic gases and char oxidation flow rates increases normal to the TPS panel above the oxygen mass flow rate, this results in the stoichiometric point that is not close to the TPS surface, but rather in the freestream. Similar observations have been noted for premixed turbulent flames. Many of the embedded TPS convective heating measurements showed a drop in heating magnitudes during the detached flame regime (Figures 17-19). This heating reduction factor was on the order of 0.3 to 0.8 (Figure 32). Flame extinction was not observed in any of the tests since the lowest ambient pressure that could be targeted was 1.9 psia. However, the flames were extremely diminished within the freestream at these lowest ambient pressures. The ground test instrumentation data showed similar observations for Artemis I post-fight reconstruction in regard to the detached flame regime[1].

The second main objective of the TVC test program was to determine the ignition heat load which would result in the onset of P50 cork combustion. The heat load is an integration of heating rate over a temporal domain. Ignition heat load was the integration of the heating rate from T+0 sec to just prior to cork ignition. Another parameter which is more conventional is the TPS ignition temperature which was not measured for the TVC test program. However, the ignition heat load and ignition temperature are directly related. Figure 33 shows the cork ignition heat load as a function of total heating rate just prior to ignition for multiple TPS samples including Hypalon coated P50 cork (orange circles in Figure 33) and bare P50 cork (white circles). This figure also shows data from Artemis I flight (red circles with DFI name labeled in Figure 33) and Green Run Hot-Fire test program (green circles)[1,5]. It can be seen in Figure 33 that the average ignition heat load for Hypalon/P50 cork was approximately 200 BTU/ft^2. There was some minor scatter in the data of +/- 50 BTU/ft^2 (shaded in pink). For the most part, bare P50 cork has a lower ignition heat load than the Hypalon coated samples. It was believed that the high-density rubber polymer paint delayed the ignition point. It was seen for multiple TVC tests, Green Run and Artemis I flight data that a large discontinuity in the convective heating rate was observed at the ignition heat load[1,5]. It should be noted that the heat load data points at 0 BTU/ft^2 pertained to the tests where cork combustion was not observed. Because this test was able to replicate cork combustion dynamics observed during Artemis I flight, this data was used to inform updated base heating models for future SLS flights in the Artemis campaign. The ignition heat load resulted in the P50 cork surface temperature reaching on the order of 1065 deg R, which was characterized by other researchers[9] and using IR pyrometry[5] during Green Run as the TPS ignition temperature.

Figure 34 shows a comparison of the cork combustion dynamics between the bare P50 cork (blue curves) and Hypalon-coated P50 cork TPS samples (red curves). Although there were only three data points, a shorter time duration to initiate cork combustion occurred with bare P50 cork as compared to the Hypalon-P50 cork TPS sample. This translated to a smaller cork ignition heat load for the bare P50 cork as compared to the Hypalon coated version (observed in Figure 33). Regarding energy release with the cork combustion process, both TPS samples led to similar convective heating jumps at the ignition point with a large scatter of data.

Figure 35 shows a qualitative trend of TVC ambient temperature as a function of peak convective heating rates. This suggested that during the cork combustion regime the gas recovery temperature was much higher (almost a factor of 2) than the lack of this combustion regime. Although gas recovery temperature was not explicitly measured, the TVC ambient temperature provided a qualitative trend of the recovery temperature. This suggested that the high cork combustion temperatures led to an increase in the convective heating rates.

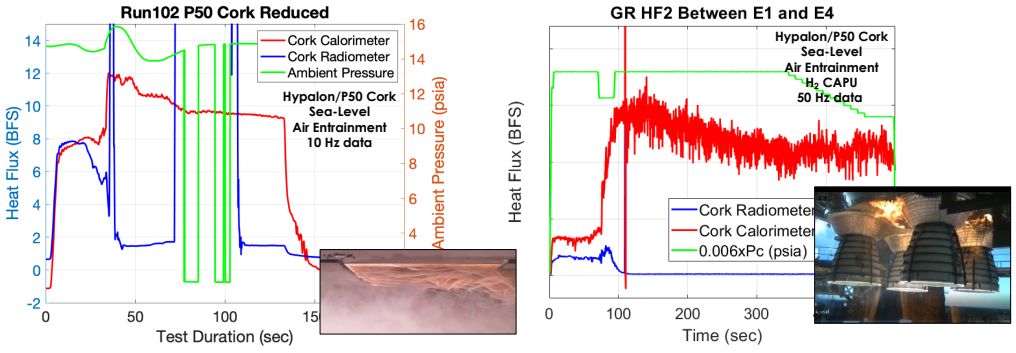

Figure 28. Embedded TPS heat flux vs. time for Run 102 (left) and Green Run Hot-Fire 2 base heat shield between E1 and E4 location[5].

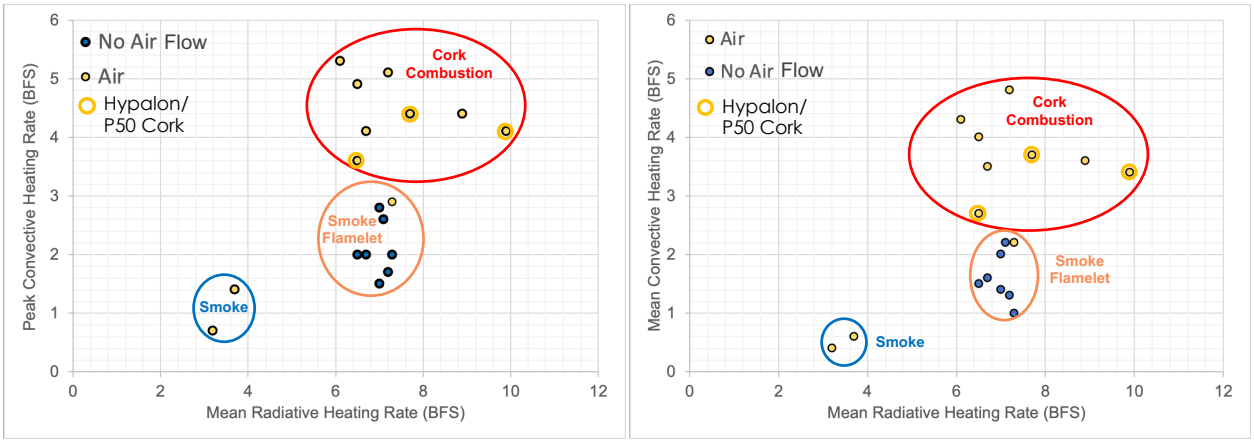

Figure 29. (left) Peak and (right) mean embedded TPS convective heat flux vs. mean input radiative heat flux

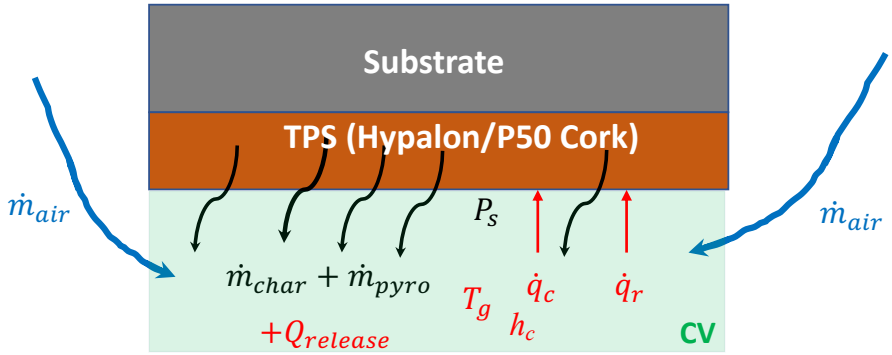

Figure 30. Schematic showing the input conditions and mechanisms behind P50 cork combustion.

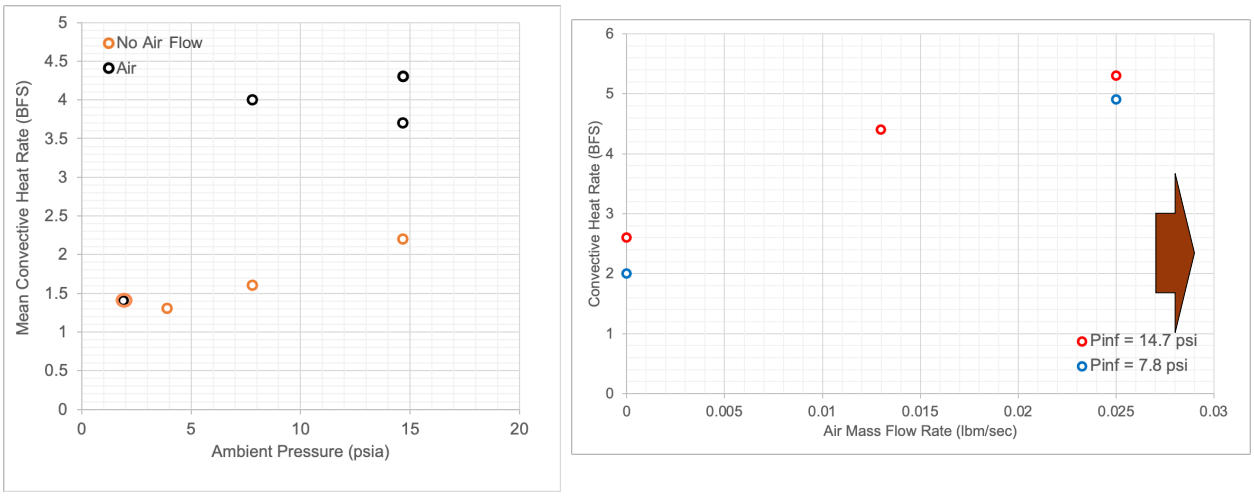

Figure 31. (left) Mean embedded TPS convective heat flux vs. ambient pressure; (right) mean embedded TPS convective heat flux vs. air mass flow rate.

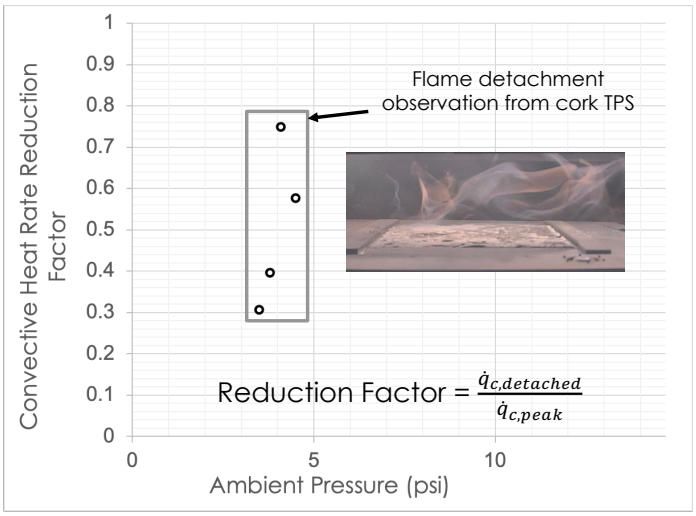

Figure 32. Embedded TPS convective heat flux reduction factor at the detached flame onset vs. ambient pressure.

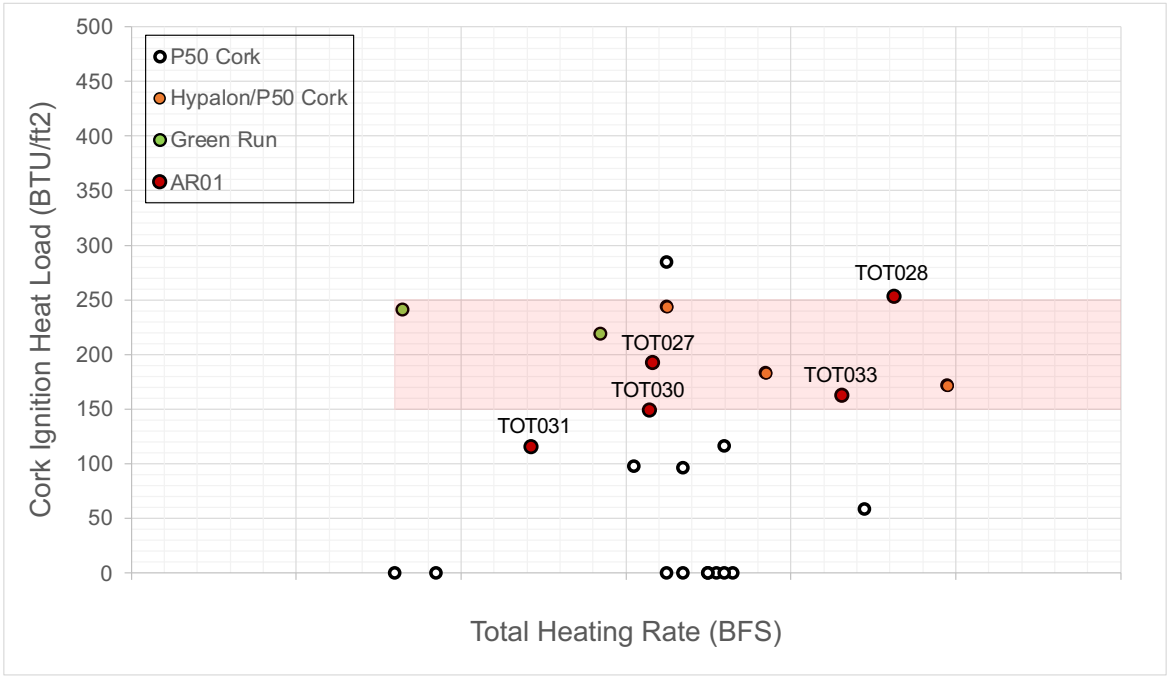

Figure 33. Cork ignition heat load vs. initial TPS total heat flux prior to cork ignition for the TVC, Green Run and Artemis I flight cases[2,3].

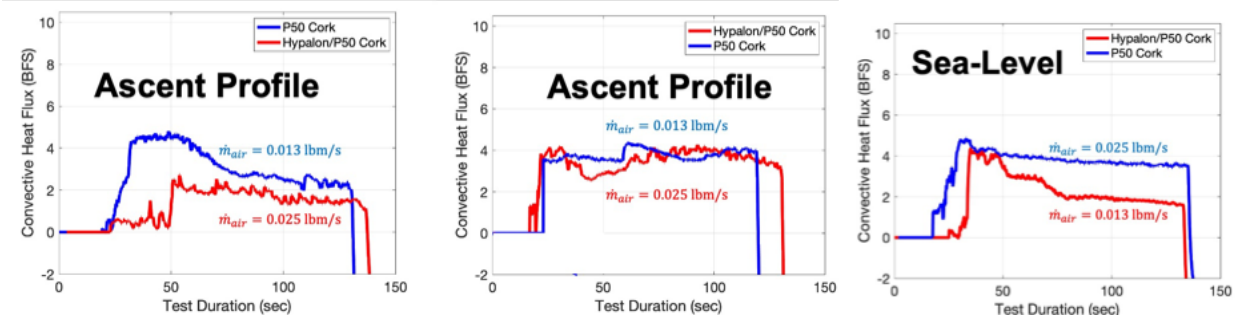

Figure 34. Convective heat flux vs. time distribution between cork combustion processes for base P50 cork and Hypalon-coated P50 cork TPS samples.

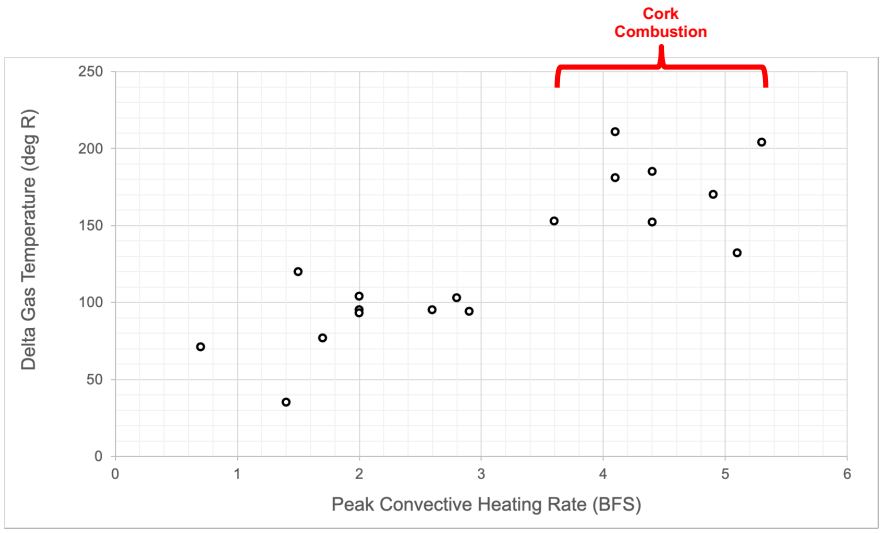

Figure 35. Gas temperature vs. embedded TPS peak convective heat flux.

Figure 36 shows the mean char formation rate and TPS mass loss as a function of mean total heating rates. It was seen that above a radiative heating target and if cork ignition heat load was achieved, the mean char formation rate was roughly twice as high as the mean rate when combustion did not occur. This suggests that a thicker char layer developed in the combustion cases where the surface convective heating was higher. Note that the mean char formation rate in the combustion cases was relatively constant under heating ranges from 9 to 14 BFS. This has implications on TPS recession and TPS design for launch vehicles and spacecraft. Figure 36 also shows that the TPS mass loss was linearly proportional to the total heating rate. Higher TPS mass loss was observed during the cork combustion regime due to a higher porosity char layer and higher convective heating rates. TPS mass loss was calculated from a weighing scale before and then after a test. Highest mass loss was observed for the Hypalon coated P50 cork samples under the cork combustion process.

Figure 37 shows visible imagery comparisons of the top-surface post-TVC test and post-Green Run Hypalon/P50 cork TPS[2]. Both the TVC test and Green Run showed similar effects of cork combustion on these TPS panels. It showed an alligator skin char appearance for all samples. More thorough look into the topology shows a honeycomb cell pattern with a relatively fixed cell diameter. For TVC Run 102, most of the Hypalon layer has burned away, leaving the charred cork underneath. For the Green Run image, the LT80 foil was seen burned and torn away, leaving the charred cork underneath within the central portion of the SLS Core Stage base heat shield[5].

Figure 38 shows comparison X-Ray CT cross section of three cork panels and the response differences between cork combustion and non-combustion TPS panels. All panels experienced the same radiative heating inputs and so the only difference was the effect of cork combustion processes on the TPS. The cork combustion panels showed a large intensity gradient between the char layer and virgin layer. The char layer of the cork combustion panels was much darker with a more pronounced gradient than the non-combustion panels. This showed that the char layer was less

dense than the non-combustion panels. The non-combustion panels showed a lighter and more diffuse gradient within the char layer suggesting a higher density char. Both the Hypalon coated and bare P50 cork panels that experienced cork combustion phenomena showed a much lower density char layer. The burning process led to a much higher convective heating and evaporation of the phenolic binder within the P50 cork which resulted in higher porosity and lower density of the char layer. This low-density char could make it more susceptible to mechanical shear erosion and augment the TPS recession rate. According to Smith et al., a P50 cork char density of less than 4.75 lb_m/ft^3 was classified as the critical failure density based on arc-jet testing[6]. For Run 102, some of the high density burned Hypalon paint was seen partially attached to the P50 cork char layer. Unfortunately, only relative density metrics could be obtained from X-Ray CT scans and absolute density values could only be obtained with CT scans of reference char samples at known densities.

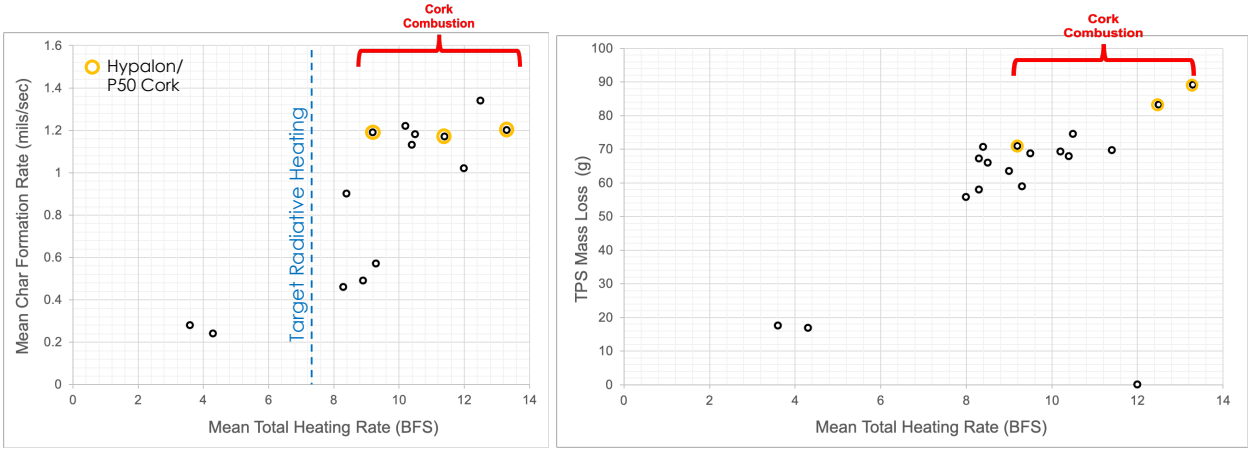

Figure 36. (left) Mean char formation rate and (right) TPS mass loss vs. embedded TPS total heat flux.

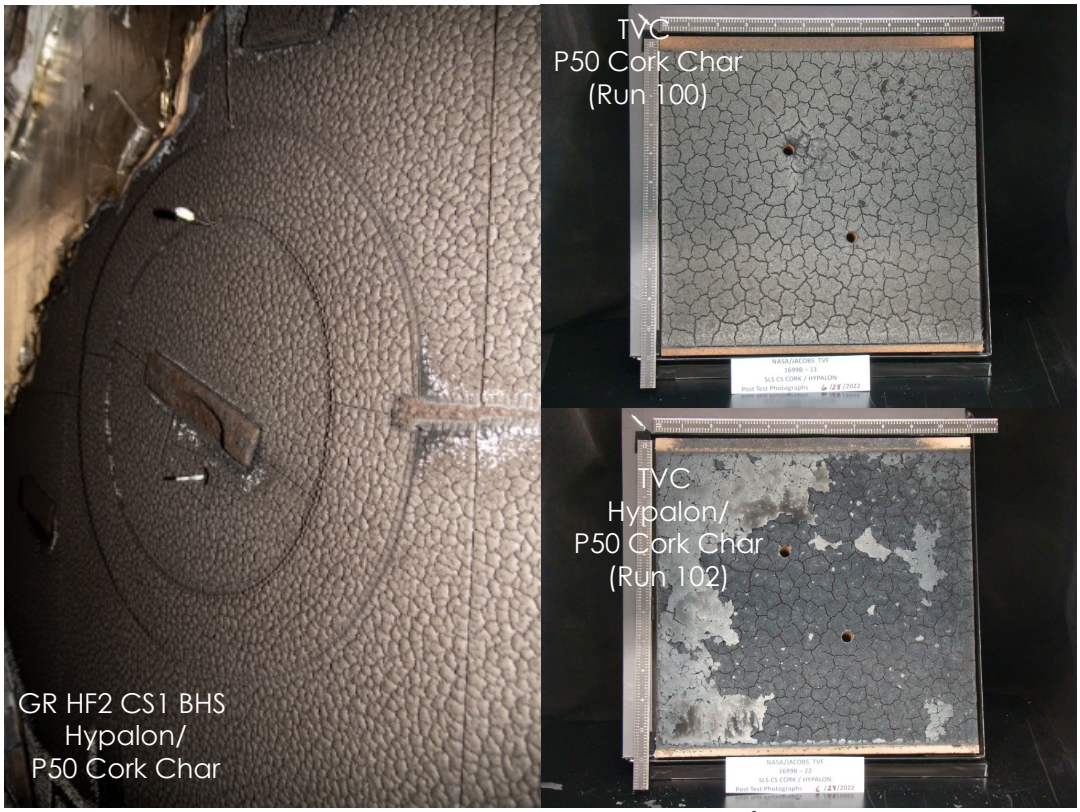

Figure 37. (left) Post-test base heat shield observations after Green Run[2] Hot-Fire 2; (right) TVC post-test TPS panel for Runs 100 and 102.

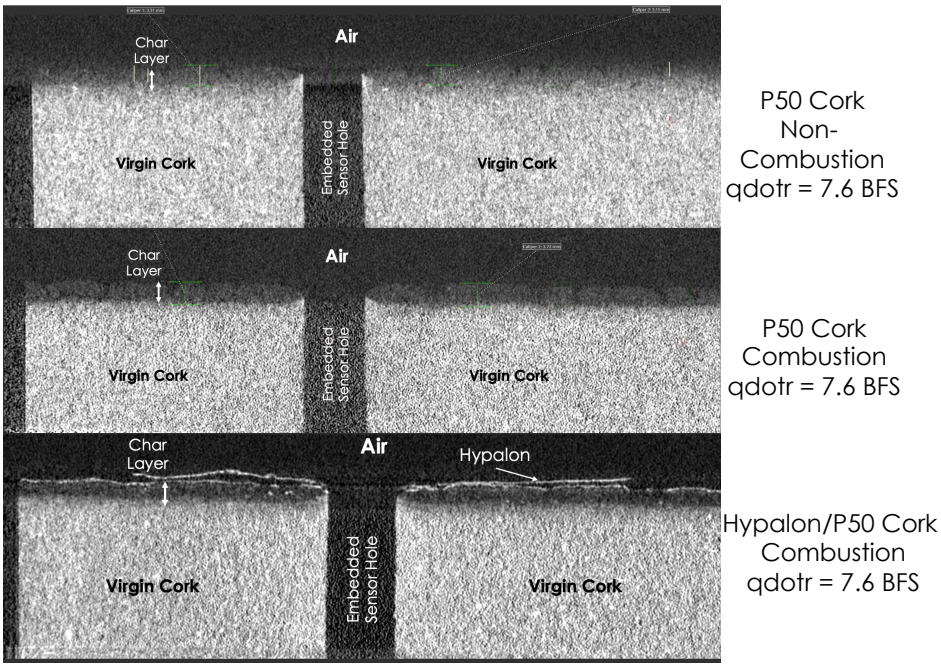

Figure 38. X-Ray CT scans of post-TVC TPS panels between non-combustion and P50 cork combustion regimes.

V. Conclusion

P50 cork environments, combustion dynamics and flow field have been characterized for changes in radiative input heating, ambient pressure, air mass flow rate, effects on coatings and test gas. This study showed the ignition heat load for various radiative heating inputs and comparisons to Green Run[5] and Artemis I flight[1,2]. The study investigated the flame propagation and quenching of P50 cork burning due to reduction in oxygen availability. This study characterized the convective heating and radiative heating environments due to the cork combustion process, and the P50 cork response which led to significant char depth and TPS mass loss. This study investigated the X-Ray CT scans and the pre- and post-TVC visible imagery of the P50 cork response due to the various induced environments and flow physics. We observed lower char density due to cork combustion than with non-combustion radiative heating effects. It was theorized that the lower char density makes the material more susceptible to mechanical shear erosion. This theory is further investigated within the Marshall Space Flight Center's Hot Gas Facility. In a nutshell, this enabled the understanding of the outgassing, ignition, cork combustion dynamics and flameout characteristics that was applied in developing Artemis I post-flight data analysis and heating model implementation for future Artemis flights. This test program data was also supplied to the HLS Program to provide insight into both ascent and reentry environments.

This investigation also showed the qualitative similarities of the TVC cork environments and response with SLS Core Stage Green Run data[5]. Most notably, the TVC test program accurately replicated cork combustion observations cited during Green Run and Artemis I flight which further assisted in flight rationale and confirmed mitigation steps. This test series along with Green Run and Artemis I flight assisted in reducing risk to the Program[1,2,5]. The novel testing methodology employed within the TVC could be used to accurately investigate the behavior of other TPS material and their associated environments for launch vehicle ascent and spacecraft re-entry low in the atmosphere. Two-phase (solid TPS and gas phase) flow environments had first come up for the SLS Program during Green Run[5] and through the TVC test program and flight[1,2], there is considerable data to understand the combustion dynamics, flow physics and TPS response. Although historically plume induced environments focused on the gas dynamics related to vehicle aerothermodynamics and aerodynamics, TPS response can induce other critical environments such as contamination, debris and as reported here, aerothermal effects. These large-scale burning environments can be

significant and as observed for Artemis I flight, can dominate the base environments during ascent[3]. The propensity of debris is only partially explored in the follow-on paper, looking at shear effects on cork char. Since the human-rated SLS vehicle has P50 cork as the main TPS ablator to protect against the extreme environments on ascent through Artemis V mission, understanding the behavior of this TPS is vital for Crew safety and mission success. Various commercial landers and upper-stage and booster vehicles for the Human Landing System (HLS) Program are currently considering P50 cork as their TPS ablators for their test flights and potentially their final TPS designs.

To further enhance the P50 cork combustion models and trends that were developed for future SLS base environment predictions, it would be ideal to measure concentration of the TPS out-gassing molecules as a function of heat rate. Using a gas chromatography – mass spectroscopy, this technique can identify compounds with low detection limits at the TPS surface. Ideal to also include a gas temperature probe and surface pressure transducer at the surface of the cork panel during the TVC test campaigns or potential future tests to more accurately estimate cold-wall heating and base aerodynamics. Raw radiometer measurements (with bias and degradation corrections) are included here, but further work on correcting these measurements due to slight changes in the FOV between the calorimeter and radiometer need to be included. This will enable more accurate chemistry, base aerodynamics and heating models specific to the cork material being used.

Appendix A: TPS Embedded Instrumentation Data Reduction Methodology

Pre-test and post-test calibration runs without the TPS sample were conducted to assist in the embedded TPS test instrumentation data reduction (Figure A1). The 5 water-cooled calorimeters on the calibration plate along with the two embedded TPS sensors provided important set-points prior to and after each TPS test run. This enabled us to determine the performance of these gauges either due to contamination or sensor drift. If there was soot contamination on the TPS embedded radiometer, cleaning of the radiometers was warranted. Cleaning of the calorimeter was not recommended by vendor and should be sent back to MEDTHERM for cleaning and recalibration due to absorptive coating requirements[8]. Since this would induce a heavy cost and schedule burden, we did not clean the calorimeters and attempted to correct for sensor drift or bias from the pre- and post-TPS calibration runs with the below equations (A1 – A6). There were two convective heating reduction approaches applied where the first approach strictly applied the reduction algorithm (red1, A5) and the second approach took an average over the reduced radiation algorithm (red2, A6). Both approaches produced similar corrected convective heating distributions, but red2 had less scatter in the data. Encouraging news was that the calorimeter and radiometer experienced low bias and sensor drift over the whole test program as observed in Figure A1 panel a, b and c. The red and blue curves in Figure A1 correspond to the TPS embedded calorimeter and radiometer measurements for the calibration runs. However, the TPS embedded radiometers did experience significant contamination during the test program. Equation A7 shows the calculation of the heat transfer coefficient using Green Run hot-fire 2 recovery temperature data during the TVC ground test cork combustion regime[1,5]. Equation A8 is the method for calculating cold-wall convective heating rates.

$$\dot{q}_{T,corr} = \dot{q}_{T,cal,TPS} - \left(\frac{\dot{q}_{T,cal,c} + \dot{q}_{T,cal,BR}}{2}\right) \quad \text{(A1)}$$

$$\dot{q}_{R,corr} = \dot{q}_{R,cal,TPS} - \left(\frac{\dot{q}_{R,cal,c} + \dot{q}_{R,cal,TL}}{2}\right) \quad \text{(A2)}$$

$$\dot{q}_{R,TPS,red} = \dot{q}_{R,TPS} - \frac{1}{t_2 - t_1}\sum_{t1}^{t2} \dot{q}_{R,corr} \quad \text{(A3)}$$

$$\dot{q}_{T,TPS,red} = \dot{q}_{T,TPS} - \frac{1}{t_2 - t_1}\sum_{t1}^{t2} \dot{q}_{T,corr} \quad \text{(A4)}$$

$$\dot{q}_{C,TPS,red1} = \dot{q}_{T,TPS,red} - \dot{q}_{R,TPS,red} \quad \text{(A5)}$$

$$\dot{q}_{C,TPS,red2} = \dot{q}_{T,TPS,red} - \frac{1}{t_2 - t_1}\sum_{t1}^{t2} \dot{q}_{R,TPS,red} \quad \text{(A6)}$$

$$h_C = \frac{\dot{q}_{C,TPS,red2}}{T_{rec} - T_w}; T_{rec} = GR\ HF2\ Data \quad \text{(A7)}$$

$$\dot{q}_{C,TPS,CW} = h_C(T_{rec} - 459.7\ R) \quad \text{(A8)}$$

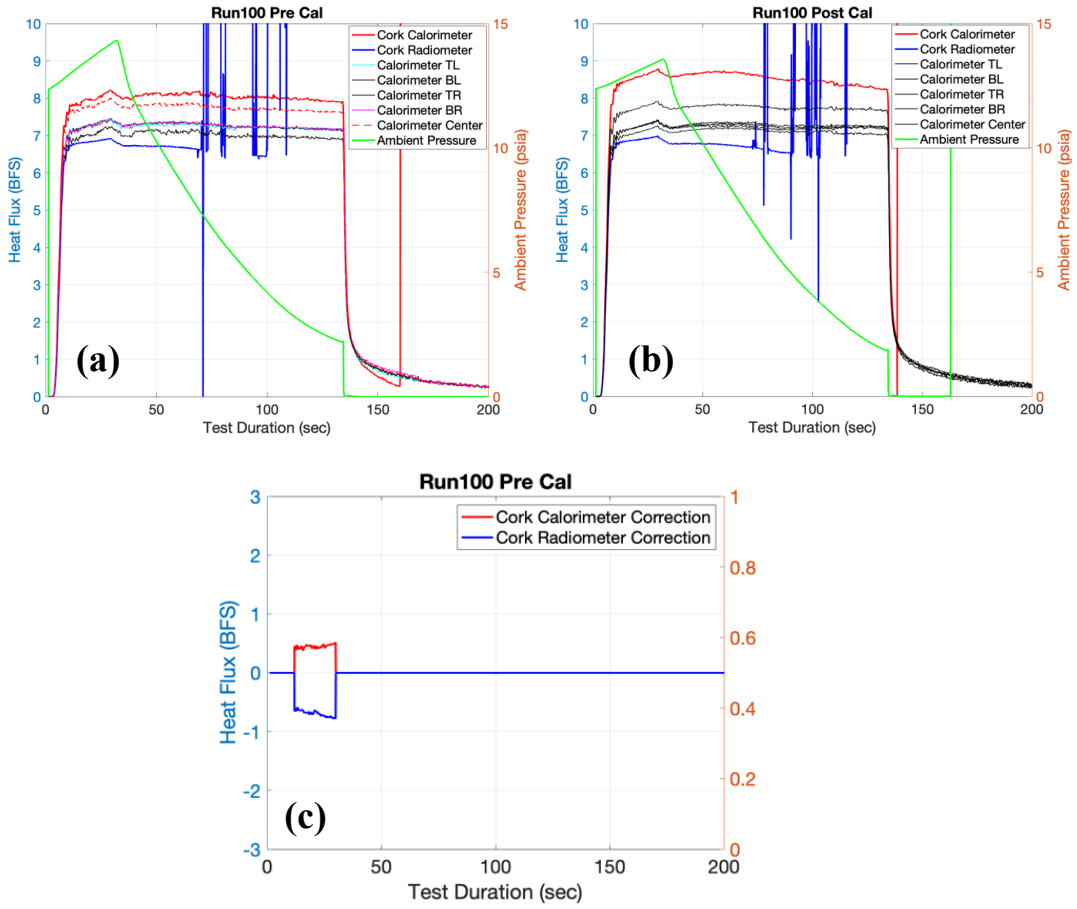

Figure A1. Run 100: (a) pre-TPS test calibration run; (b) post-TPS test calibration run and (c) sensor correction

Acknowledgements

Thanks to the efforts of the technical staff within the NASA Marshall Space Flight Center's Aerosciences Branch such as Dr. Chris Morris and Brandon Mobley for data review and flow physics insight and the Nonmetallic Materials and Space Environmental Effects Branch for access to the thermal vacuum chamber, testing, data reduction and development of the TPS specimens. Contributions from the Damage Tolerance Branch in access to their facilities and X-Ray systems have been extremely beneficial in evaluating the TPS response and characterization. Valuable guidance and assistance from Darrell Davis of the MSFC Thermal Analysis and Control Branch was also provided. This testing was supported by Michael Alldredge and Eric Vanderslice of the SLS Stages Office and Janet Sisk of the Structural Design and Analysis Division within the MSFC Vehicle and Spacecraft Department.

References

[1]Mehta, M., B.L. Mobley and S.D. Smith., "Space Launch System Base Aerothermodynamics Post-Flight Reconstruction for Artemis I," *AIAA SCITECH 2024 Forum*, American Institute of Aeronautics and Astronautics, 2024. https://doi.org/10.2514/6.2024-0256

[2]Mehta, M. and T.B. Steva, "Space Launch System Base Aerodynamics Post-Flight Reconstruction for Artemis I," *AIAA SCITECH 2024 Forum*, American Institute of Aeronautics and Astronautics, 2024. https://doi.org/10.2514/6.2024-0257

[3]Morris, C.I. (2015), "Space Launch System Ascent Aerothermal Environments Methodology", *53rd AIAA Aerospace Sciences Meeting, AIAA SciTech*, (AIAA 2015-0561), Kissimmee, FL. https://doi.org/10.2514/6.2015-0561

[4]Scott, C.F. and J.A. Inman, "SCIFLI Airborne Observation of the Hayabusa2 Sample Return Capsule Re-Entry", *AIAA AVIATION 2022 Forum,* American Institute of Aeronautics and Astronautics, 2022, https://doi.org/10.2514/6.2022-3798

[5]Mehta, M., C.I. Morris, B.L. Mobley and T.L Prickett., "Space Launch System Core Stage Green Run Base Heating: Anomaly, Mitigation and Flight Redesign," *AIAA SCITECH 2023 Forum*, American Institute of Aeronautics and Astronautics, 2023. https://doi.org/10.2514/6.2023-0644

[6]Smith, E., B. Lamb, R. Beck and E. Fretter (1992), "Thermal/Ablation Model of Low-Density Cork Phenolic for the Titan IV Stage I Engine Thermal Protection System", AIAA 92-2905, Nashville, TN

[7]Mehta, M., Dufrene, A. T., Seaford, M., and Knox, K., "Space Launch System Base Heating Test: Environments and Base Flow Physics," *54th AIAA Aerospace Sciences Meeting*, American Institute of Aeronautics and Astronautics. https://doi.org/10.2514/6.2016-0547

[8]MEDTHERM Corporation, "64-Series Heat Flux Transducers and Infrared Radiometers for the Direct Measurement of Heat Transfer Rates", Bulletin 118, MEDTHERM Co, Huntsville, AL, 2002.

[9]Sen, Ali & Van den Bulcke, Jan & Defoirdt, Nele & Van Acker, Joris & Pereira, Helena. (2014). Thermal behavior of cork and cork components. Thermochimica Acta. 582. 10.1016/j.tca.2014.03.007.

[10]Sakraker, I., Chazot, O. & Carvalho, J.P. Performance of cork-based thermal protection material P50 exposed to air plasma. *CEAS Space J* **14**, 377–393 (2022). https://doi.org/10.1007/s12567-021-00395-z